https://doi.org/10.5194/egusphere-2026-6438
Preprint. Discussion started: 11 November 2026
© Author(s) 2026. CC BY 4.0 License.

On the direct radiative impact of upper tropospheric aerosol particles

Holger Tost[1], Matthias Kohl[2], J. Moritz Menken[3], Matthias Nützel[3,4], Laura Stecher[3,x], Domenico Taraborrelli[5], and Ryan Vella[1,2,*]

[1]Institute for Atmospheric Physics, Johannes-Gutenberg University Mainz, Germany
[2]Max Planck Institute for Chemistry, Mainz, Germany
[3]Deutsches Zentrum für Luft- und Raumfahrt, Institut für Physik der Atmosphäre, Oberpfaffenhofen, Germany
[4]Meteorologisches Institut München, Ludwig-Maximilians-Universität München, Munich, Germany
[5]Institute of Climate and Energy Systems - Troposphere (ICE-3), Forschungszentrum Jülich GmbH, Jülich, Germany
[*]now at Institute for Atmospheric and Climate Science, ETH Zürich, Zurich, Switzerland
[x]now at Centre for Atmospheric Science, University of Cambridge, United Kingdom

Correspondence: Holger Tost (tosth@uni-mainz.de)

Abstract. Despite the largest aerosol mass being located in the lower troposphere, the aerosol content of the upper troposphere (UT) plays an important role in the atmospheric radiation budget, both via direct and indirect aerosol-radiation interactions. The UT already has been identified as a highly sensitive region for the energy budget. This study analyses those interactions in this altitude relevant for climate change processes.

For this purpose, global chemistry-climate model simulations are presented focussing on aerosol-radiation interactions. Employing a newly developed, highly flexible scheme for aerosol optical properties, the simulations depict the role of UT aerosol particles in the Earth's radiation budget. First, the fractional contribution of the UT aerosol to the total extinction is quantified, and the compounds relevant for the aerosol extinction are identified. It is shown, that the UT extinction contributes to more than 10 % in the global average, and that aerosol water is the most important component for the extinction. The sensitivity of the radiation budget to UT aerosols is analysed by scaling experiments of the upper tropospheric extinction. It is shown that the modified extinction results in significant changes in the radiative fluxes at the surface and throughout the whole atmosphere. A doubling of the extinction in the UT leads to a surface radiative disturbance of a global mean value of approximately 0.1 W/m^2. Therefore, an increase in UT aerosols due to direct emissions, transport from near surface sources or space debris could result in a significant modification of the Earth's radiation budget.

1 Introduction

Aerosol particles are known to be important players in the global radiation budget of the Earth. The total effect from direct aerosol radiation interactions is estimated to be around -2.4 W/m^2 (Matus et al., 2019), which is substantially larger than the anthropogenic direct aerosol effect that is estimated to be $\sim$ -0.4 W/m^2 (e.g., Forster et al., 2021). Consequently, anthropogenic aerosol particles play only a secondary role in the total atmospheric extinction and absorption. Nevertheless, the influence of human-kind on the atmospheric extinction is already offsetting a part of the greenhouse gas induced warming

https://doi.org/10.5194/egusphere-2026-6438
Preprint. Discussion started: 11 November 2026
© Author(s) 2026. CC BY 4.0 License.

(e.g., Forster et al., 2021). Furthermore, the aerosol-cloud-radiation interactions are generally a factor of two to three larger on the global scale than the direct aerosol-radiation interactions. However, in certain areas of the atmosphere, there are no clouds (deserts, upper atmosphere), such that the direct aerosol-radiation interactions are still an important factor in the climate system. Additionally, the level of uncertainty for direct aerosol-radiation interactions is assumed to be lower compared to aerosol-cloud-radiation interactions due to the more comprehensive interactions and complex mechanisms in the aerosol-cloud interactions.

Even though the majority of the atmospheric aerosol load is located near the main sources, i.e., in the planetary boundary layer (PBL), also a non-negligible portion of aerosol particles of various sizes are found in the upper troposphere and the stratosphere. Junge and Manson (1961) already pointed out, that there is a substantial layer of stratospheric aerosols, which are nowadays known to originate mostly from OCS (carbonyl sulfide) transport from the Earth's surface and subsequent chemical conversion to gaseous sulfuric acid (H_2SO_4), which can form new particles, that have implications for the radiative balance (e.g., Brühl et al., 2012). An excellent review about the stratospheric aerosol layer and its origin, observations and implications is provided by Kremser et al. (2016).

In addition to the Junge layer, there is also an increasing interest in upper tropospheric (UT) aerosol composition and load (e.g., Brock et al., 1995; Borrmann et al., 2010; Williamson et al., 2019; Weigel et al., 2021; Williamson et al., 2026; Kohl et al., 2026), because in this region natural and anthropogenic processes (due to transport from near surface emission sources) jointly shape the composition and size distributions of the aerosol characteristics. Several studies of upper tropospheric aerosols are either related to the Asian monsoon and the Asian Tropopause Aerosol Layer (ATAL) (e.g., Mahnke et al., 2021; Pan et al., 2025) or to the Amazon (e.g. Curtius et al., 2024) and mostly deal with new particle formation. However, additional studies also focus on the fate of those freshly formed particles (e.g., Williamson et al., 2026; Hernández Pardo et al., 2026), analysing either the microphysical properties or their transport patterns.

For the simulation of the interactions of UT aerosol particles with radiation, the optical properties of those aerosol particles are required. While first studies mainly show the strong correlation of particle size and number density to extinction (e.g., Waggoner et al., 1981), later findings analyse extinction and other optical effects for single particles (e.g., Walker et al., 2013) in the laboratory or as column values either from sun photometers (e.g., AERONET, Giles et al. (2019) and references therein) or satellite products (e.g., Remer and Kaufman, 1998; Remer et al., 2005; Levy et al., 2007). Theoretical approaches follow Mie-theory (Mie, 1908), as the particles are usually in the size range of the visible or infrared wave lengths relevant for the Earth's atmosphere. Usually, simplifications concerning the shape of the particles (often spheres) and the mixing states (internal versus external mixing states) (e.g., Hess et al., 1998) are assumed to efficiently solve the equations numerically to obtain extinction, absorption (or Single Scattering Albedo SSA) and the direction of scattering (forward or backwards or the full phase function, summarised in the ASymmetry Factor, ASF).

Those aerosol optical properties have been determined with various approaches in the past decades, continuously improving the algorithms and representations of individual particles based on novel theoretical approaches, updated experiments and improved algorithms. This progress is reviewed e.g. by Liu et al. (2023), which on the one hand explain the background (scattering matrix and Mueller matrix) and the resulting quantities (extinction, absorption, optical thickness) as well as the spectral

https://doi.org/10.5194/egusphere-2026-6438
Preprint. Discussion started: 11 November 2026
© Author(s) 2026. CC BY 4.0 License.

dependence of those quantities. Furthermore, modern approaches of the calculation of the optical properties of atmospheric aerosols can be found in their work, which go well beyond the approaches used for the calculations used in this study. A slightly more simplified approach for optical properties is described in Emde et al. (2016) using the libRadtran model, which also falls back to code for the Mie calculations from Wiscombe (1980). In addition to approaches trying to determine the optical properties from physical principles also data driven methods have been established in the past. Those approaches either use directly measured data and apply machine learning methods to constrain the relations between refractive indices and particles size and wavelengths or "learn" those relations by using established parameterisations (e.g., Kumar et al., 2024). Even though the ML methods are efficient, the usage of lookup tables is as fast in the operation of chemistry-climate models, such that neural networks only start to outperform table lookups in high dimensionality parameter space, such as an explicit treatment of "core" and "shell" contributions of mixed aerosol particles (as described by e.g., Bohren and Huffman, 1998).

This study follows the more traditional approach with pre-calculated lookup tables for aerosol extinction single scattering albedo and asymmetry factors due to computational performance. In the following section of the manuscript the applied modelling sytem is described with a focus on the novel submodel for aerosol optical properties (AOP) included in the Modular Earth Submodel System (MESSy, Jöckel et al., 2005). In the results section, the model results are shortly evaluated and compared to a previous model version. Afterwards, the following key questions are analysed:

- What is the contribution of upper tropospheric aerosols to extinction and which compounds dominate the radiative effects?
- How do UT aerosols affect climate by direct aerosol-radiation interactions and how sensitive is the surface climate to changes in UT extinction?
- What is the role of organic aerosols in the optical properties and radiative impact in the upper troposphere down to the surface?

Finally the results are summarised and some implications for future studies are briefly mentioned.

2 Model description and simulation configuration

For this study the chemistry climate model EMAC (ECHAM/MESSy Atmospheric Chemistry) has been extended and applied. EMAC is a numerical chemistry and climate simulation system that includes sub-models describing tropospheric and middle atmosphere processes and their interaction with oceans, land and human influences (Jöckel et al., 2010). It uses the second version of the Modular Earth Submodel System (MESSy2) to link multi-institutional computer codes. The core atmospheric model is the 5th generation European Centre Hamburg general circulation model (ECHAM5, Roeckner et al., 2006). The physics subroutines of the original ECHAM code have been modularized and reimplemented as MESSy submodels and have continuously been further developed. Only the spectral transform core, the flux-form semi-Lagrangian large scale advection scheme, and the nudging routines for Newtonian relaxation are remaining from ECHAM. For the present study we applied EMAC (MESSy version 2.55.1).

https://doi.org/10.5194/egusphere-2026-6438
Preprint. Discussion started: 11 November 2026
© Author(s) 2026. CC BY 4.0 License.

2.1 Model description

The EMAC model contains a variety of process submodels for atmospheric physics and the chemical composition of the atmosphere, including gas phase chemistry as well as aerosol processes and cloud processing of air masses. A comprehensive list of submodels used can be found in the accompanying supplement; only the most relevant processes and new developments are described in this manuscript.

2.1.1 Aerosol representation

Aerosol microphysics and the chemical composition of aerosol particles are described with the GMXe submodel (Global Modal aerosol eXtEnsion, Pringle et al., 2010). GMXe represents the aerosol size distribution with the help of 4 hydrophilic and 3 hydrophobic lognormal modes, including an internal mode width parameter (standard deviation) of 1.59 for nucleation, aitken and accumulation modes and 2.0 for the coarse modes. The processes contained are new particle formation, coagulation and respective changes in the size distribution. Condensation and exchange of inorganic gaseous species are determined based on the thermodynamic equilibrium model ISORROPIA-2 (Fountoukis and Nenes, 2007). Considered compounds in the aerosol are sulphate, nitrate, ammonium, water, desert dust, sodium, chloride, black carbon and organic carbon. The latter compound is split up in biogenic secondary organics and primary emitted organic carbon from biomass burning and anthropogenic activites. Even though secondary organic aerosols (SOA) and non-equilibrium processes in the aerosol phase can be explicitly considered, (e.g., Rosanka et al., 2024), a more simplified approach has been chosen in this study, by directly emitting SOA compounds based on emission fluxes from the AEROCOM project (Mann et al., 2014). This aerosol representation has been used in numerous studies and proven its applicability (e.g., Abdelkader et al., 2023; Kohl et al., 2023; Tost, 2017; Pozzer et al., 2015).

2.1.2 Radiative transfer

This study uses the standard radiation scheme of ECHAM5 (see Roeckner et al., 2006), which has been modified to account for upgrades (Thomas, 2008) from the original code version. Furthermore, the inclusion of aerosol optical properties from interactive aerosol species has been added to the radiation code, to take the aerosol-radiation interactions directly into account. Additionally, using the radiation infrastructure of MESSy (Dietmüller et al., 2016; Nützel et al., 2024), multiple calls to the radiation for diagnostic purposes are utilised in this study.
Note, that the optical property calculations allow for much more flexibility in coupling with different radiation schemes, i.e., the AOP submodel can also be applied with the PSrad scheme (Pincus and Stevens, 2013).

2.1.3 Aerosol optical properties

A new process submodel for Aerosol Optical Properties (AOP) has been developed based on the original AEROPT submodel described in Dietmüller et al. (2016), which determines the optical properties (namely extinction, single scattering albedo and asymmetry factor) of aerosol particles for multiple compounds and wavelengths. In contrast to its antecedent, the new scheme

https://doi.org/10.5194/egusphere-2026-6438
Preprint. Discussion started: 11 November 2026
© Author(s) 2026. CC BY 4.0 License.

offers various ways and parameterisations, how the optical properties are calculated. Additionally, the new AOP submodel is applicable for flexible aerosol size distributions and more easily expandable for additional compounds with different optical properties, e.g., meteoric particles or different types of dust (road dust versus desert dust). Both an option for pre-generated lookup-tables as well as online calculations are implemented; however, the lookup-tables are by far more computationally efficient. Consequently, these tables should be generated ahead of a 3D global simulation by application of the AOP capabilities to be used as a box model. The lookup-tables only contain the optical properties, namely the extinction, the single scattering albedo and the asymmetry factor in a three dimensional parameter space provided by the Mie size parameter and the complex refractive index.

The optical properties are first calculated on a pre- or user-defined set of wavelengths (using a specific spectral resolution), and are then later mapped to the wavelength bands of the applied radiation code. This mapping to the required wavelength-bands is done interactively with respective weights calculated online during the model simulation, such that a high degree of flexibility in the spectral resolution can be achieved, i.e., a coupling to different radiation schemes is straight-forward and is performed automatically, if either the wavelength bands are provided as namelist parameters or an online variable.

To determine the corresponding refractive indices of the individual single-compound aerosol species of the wavelength basis on which the optical properties are calculated, tables with a high spectral resolution for each compound are incorporated into the model. Alternatively, fitted functions for the refractive wavelengths (higher order polynomials) can be utilised as well as external data files (either in wavelength or wavenumber representation). The scheme is easily extendable in terms of adding additional compounds, e.g., brown carbon or volcanic ash. The corresponding refractive indices have to be incorporated in the model code directly or can be read in from csv values, and the extension efforts are minimal, in contrast to the previously used AEROPT submodel, where both the refractive indices and optical properties have been stored in a combined lookup-table with substantially less flexibility. Additionally, extra compounds for the optical calculations could only be added with tremendous effort as all connections have been hardcoded. The calculations of the optical properties depend on three parameters, i.e., the dimensionless Mie size parameter (i.e., $x = 2 \cdot \pi \cdot r_p/\lambda$, with r_p being the aerosol particle radius and λ the wavelength of the interacting radiation) and the complex refractive index for each aerosol particle. To determine the refractive indices, mixing assumptions (internally (volumetric averaged) versus externally mixed) are applied for each individual mode. To determine the Mie size parameter a lognormal distribution of aerosol particles with the same mode width σ as for the input delivering aerosol scheme is taken into account, i.e., a weighted average of 49 points in the size distribution with a given mode mean radius for the optical properties is calculated. For the Mie-calculations parameterisations from Wiscombe (1980) (MIEV0), Du (2004) for spherical particles and Bohren and Huffman (1998) for both spherical particles (BHMIE) and coated spheres (BHCOAT) are implemented and can be used either for online calculations or the construction of pre-calculated lookup-tables, which are read by the model in the initialisation stage of a simulation. The pre-calculated lookup tables have to be calculated for each required mode width of the respective aerosol size distributions.

During the development of this module, several ideas have been derived from the "mie" tool of the LIBRADTRAN (Emde et al., 2016), whereas the code for the parameterisations has been extracted from the respective documentations, as cited above. The pre-calculated lookup-tables are read in the initial phase of a GCM simulation, and afterwards a nearest neighbour lookup

https://doi.org/10.5194/egusphere-2026-6438
Preprint. Discussion started: 11 November 2026
© Author(s) 2026. CC BY 4.0 License.

for the three dimensional parameter space of mie size parameter, and real and imaginary part of the refractive index of the aerosol mixture is performed. This is subsequently performed for all aerosol modes. After determining the optical properties for one individual particle, the final values are obtained by scaling with the aerosol number concentrations and respective weighting for the SSA and ASF.

In addition to the online calculated optical properties of interactive aerosols using one of the EMAC aerosol submodels, two aerosol climatologies are implemented in the AOP submodel, namely the spectral climatology from Tanre et al. (1984), which uses the online relative humidity for water uptake of fixed aerosol concentrations for 5 aerosol species and the observation derived climatology from Kinne et al. (2013). Both of those climatologies are specifically adapted to the respective radiation scheme, described above.

Multiple sets of aerosol optical properties can be calculated simultaneously, e.g., utilising different refractive index values, different mixing assumptions or taking only selected compounds or parts of the particle spectrum of the aerosol into account. Furthermore, the AOP submodel contains functionalities to merge different sets of aerosol optical properties, e.g., an option to merge the properties of the CCMI stratospheric aerosol climatology (see Morgenstern et al., 2017) with either a tropospheric climatology or interactively calculated optical property dataset. This merging can be operated on model levels, pressure or arbitrary vertical coordinates (as long as they are monotonic in the region of merging). Additionally, options for scaling of the different optical datasets are included as well as an addition of two optical datasets, e.g., in case a specific compound is not considered in an online calculation and should be added from a climatology as an external mixture. This merging can be operated iteratively, such that also a merged dataset can be used in a subsequent merge to create an additional merged dataset.

2.2 Simulation configuration

EMAC has been applied in the resolution T42L90MA, i.e., with a spectral truncation of T42 (corresponding to a quadratic Gaussian grid of approx. 2.8 by 2.8 degrees in latitude and longitude) with 90 vertical hybrid pressure levels up to 0.01 hPa. A full chemistry-climate configuration (see Jöckel et al., 2016) utilising process submodels including gas phase chemistry (Sander et al., 2019), aerosol processes (Pringle et al., 2010; Tost, 2017), cloud chemistry and scavenging (Tost et al., 2006, 2010), and emission (Kerkweg et al., 2006b) and deposition (Kerkweg et al., 2006a) processes has been enabled. The emission data represent conditions for the year 2010. The simulation period is limited to three years after spin-up, as the sensitivity of radiative fluxes is the focus of this study, but not its multi-year variability. Note that aerosol-cloud interactions are not taken into account in this study. The resulting aerosol distribution compares well with in-situ observations and its implications in the troposphere and the UT (Pringle et al., 2010; Pozzer et al., 2015; Abdelkader et al., 2023). Emission data originate from the CCMI2 project (Plummer et al., 2021). Furthermore, the meteorology in EMAC is nudged towards ERA5 data (Hersbach et al., 2020).

Aerosol radiation interactions can use the interactively calculated aerosol distribution and from this the well established previous approach of aerosol optical properties as described in Dietmüller et al. (2016) and Pozzer et al. (2015). In the current simulation, the Tanre et al. (1984) climatology for the aerosol optical properties in the troposphere is merged with the CCMI aerosol climatology from Morgenstern et al. (2017) for the optical properties of aerosols in the stratosphere. This merged dataset is fed into the radiation code to determine the prognostic heating rates in the simulations. Additionally, multiple diag-

https://doi.org/10.5194/egusphere-2026-6438
Preprint. Discussion started: 11 November 2026
© Author(s) 2026. CC BY 4.0 License.

nostic calls to the radiation scheme are performed, which use modified and merged datasets for aerosol optical properties from the new AOP submodel to investigate the sensitivity of enhanced and weakened aerosol extinction in the UT on the atmospheric radiation budget. Furthermore, sensitivities on the role of the refractive indices of organics, especially a distinction between primary and secondary biogenic organics are analysed using a second set of aerosol optical properties from the same simulation in which SOA particles utilise the same wavelength dependent refractive index dataset as the remaining organic carbon.

To facilitate an analysis of those sensitivities, the AOP submodel is utilised with multiple aspects described in Sect. 2.1.3, namely determining multiple sets of optical properties and enhancement or reduction of specific parameters, e.g., the extinction in a specific altitude region between 300h Pa and 80 hPa, which is supposed to cover the whole UT and slightly beyond. However, the transport and distribution of the aerosol particles are consistent with the underlying dynamics, such that the aerosol optical properties are spatially and temporally highly variable in the UT region and only the extinction is modified as a whole by scaling. This would correspond to a modification of the particle numbers without changing neither the shape of the size distribution nor the chemical composition.

With each set of optical properties a diagnostic call to the radiation scheme is performed to analyse the impact on the radiation budget of the UT and the regions above and below. Consequently, for all compared datasets the meteorological conditions and atmospheric composition are identical (i.e., temperature, pressure and wind fields, which are also nudged towards ERA5 reanalysis data, as well as clouds and their properties, but also water vapour and radiatively active gases and aerosol particles), such that the differences in the radiation fluxes originate solely from the aerosol optical properties.

For comparison of the AOP and the AEROPT scheme, online diagnostic calls with interactive aerosols to each of the calculation of the optical properties are conducted in parallel driven by the same aerosol fields are conducted.

3 Results and Discussion

3.1 Aerosol optical properties

3.1.1 Evaluation of AOP versus AEROPT and MODIS

To analyse the performance of the new AOP submodel, the results are directly compared with the previous model representation as well as with MODIS (Moderate-resolution Imaging Spectroradiometer) aerosol data. The temporal mean value for the column total aerosol extinction (Aerosol Optical Thickness, AOT) at a wavelength of 550 nm is calculated diagnostically, both with the new and the old scheme for aerosol optical properties, which is depicted in Fig. 1. Panel a) depicts the mean value from the three evaluated years of simulation data. Panel b) provides the corresponding data combined from the MODIS instruments onboard AQUA and TERRA using the Deep Blue products (Levy et al., 2010, 2013). Even though the model shows some discrepancies compared to the MODIS product, the general features of elevated aerosol extinction are properly represented. However, the effect of the dust load in the model is too high with pronounced maxima in Northern Africa, the Arabian peninsula, parts of Central Asia and Australia, namely in the well-known dust source regions. On the other hand simulated AOT in China is underestimated, most likely due to too low anthropogenic primary and secondary aerosol species.

https://doi.org/10.5194/egusphere-2026-6438
Preprint. Discussion started: 11 November 2026
© Author(s) 2026. CC BY 4.0 License.

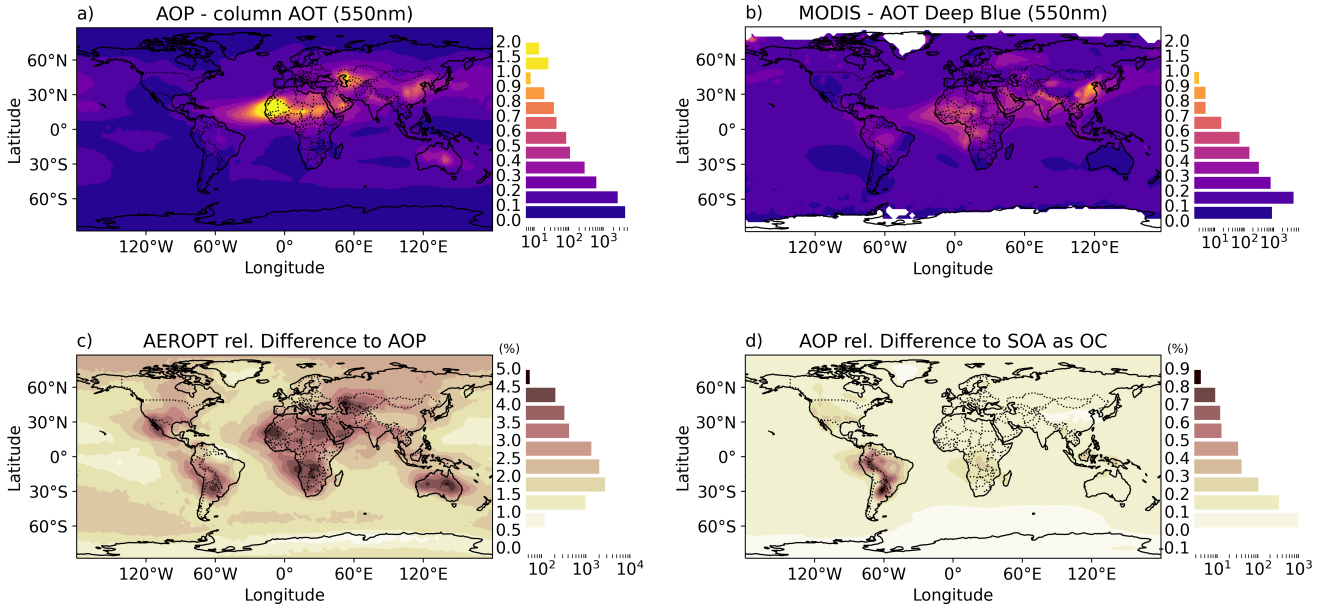


Figure 1. Panel a) shows the column aerosol optical thickness (AOT) at a wavelength of 550 nm calculated with the AOP submodel. Depicted is a three-year mean of conditions for 2010. The color bar also shows a logarithmic frequency distribution how often each AOT value occurs. Panel b) depicts a similar picture for the MODIS Deep Blue product for the year 2010. Panel c) displays the percentage difference of the new AOP submodel to the predecessor optical property model AEROPT (i.e., shown is (AEROPT - AOP)/AOP. In panel d) the relative difference of the modified refractive indices for organics and less absorbing properties for SOA are shown for the lowest shortwave radiation band (instead of the 550 nm) (AOP with values for one OC species - AOP with distinguished optical properties for organic compounds.

Furthermore, a small underestimation in the Amazon and Central Africa, either due to underestimated biomass burning or SOA species is also simulated. Some of those characteristics have already been analysed and investigated by Pozzer et al. (2015) and the overestimated dust load results most likely from a too-strong wind driven emission flux.

Comparing the new AOP calculations with the previous aerosol extinction scheme AEROPT (panel c) of Fig. 1), as described in Dietmüller et al. (2016), the differences between the new and the old algorithm are minor (smaller than 5 %, with the more frequent occurrences on the order of 2 to 3 %). Even though the same principles have been utilised in both model approaches, the discretised lookup-tables for the aerosol optical properties have a different resolution, i.e., the new scheme uses only one lookup-table per mode width, whereas in the old scheme, different lookup-tables for Aitken and accumulation mode have been created with different bounds in the Mie size parameter. Consequently, the small differences between the two model versions can be attributed to a slightly altered lookup-table. Additionally, there are some differences in the interpolation of the refractive indices, used as input for the respective species, from which the mean refractive index of the internally mixed particles is calculated. The deficiencies compared to the satellite observations are not a consequence of the optical property calculations, but the aerosol emissions and distributions. However, the slight reduction of the AOP values compared to the AEROPT column

https://doi.org/10.5194/egusphere-2026-6438
Preprint. Discussion started: 11 November 2026
© Author(s) 2026. CC BY 4.0 License.

extinction moves closer toward the satellite observations.

When analysing the refractive indices for particulate organic carbon (OC) in the AEROPT code, refractive indices according to Sutherland and Khanna (1991) have been applied for all types of OC. However, those refractive indices originated from measurements of biomass burning OC, therefore not being representative for SOA. Consequently, in the AOP scheme for organic carbon optical properties the default is to separate SOA from OC from burning products (fossil or biomass burning). SOA compounds utilising refractive indices as utilised in the CESM2 model for hydrophilic OC (e.g., Liu et al., 2016), whereas the burning OC applies refractive indices from Sutherland and Khanna (1991). The differences in AOT due to the alternative, more realistic SOA refractive indices leads to a reduction of the AOT as depicted by the positive difference of AOT in Fig. 1d, compared to the previous approach utilising the Sutherland and Khanna (1991) refractive indices for all organic compounds. This is mostly due to the less absorbing properties of SOA compared to OC from biomass burning in the short wave (<500 nm) spectral range. Note, that for this analysis the lowest band of the radiation calculations is used instead of a reference wavelength of 550 nm, as the differences in the refractive indices are only significant at shorter wavelengths. The impact of the modification of the refractive indices for SOA components is analysed in detail in Sect. 3.4.

3.1.2 UT aerosol extinction

The UT is far away from most of the primary aerosol sources as well as from aerosol precursor emissions sources (except aviation and rocket launch emissions, meteoric material and space debris). Due to the higher sedimentation velocity of the larger particles, mineral dust and sea salt are not the dominating compounds, when analysing the extinction in the UT. Also the total UT extinction is substantially smaller than the total column extinction. Fig. 2 depicts the zonal mean of the time averaged extinction on a pressure grid between 50 and 350 hPa. The stronger extinction signals originate from the lower part of the region, i.e., the troposphere. An obvious gradient with altitude can be detected, such that the aerosol extinction close to the tropopause (red line) is relatively low. Note, that in this study there is no explicit stratospheric aerosol representation calculated as e.g., by Kohl et al. (2026), such that the extinction of the Junge layer is substantially underestimated. Consequently, this study deals mostly with the UT aerosol, and does not comprise the whole UTLS region. For the consideration in the radiation driving the dynamics this effect is included making use of the *merging* capabilities of the model, merging tropospheric (from the Tanre et al. (1984) climatology and stratospheric aerosol (from CCMI, Morgenstern et al., 2017) optical properties for a consistent treatment.

A distinct maximum can be seen at 35°N, which represents the Tibetan plateau and effects of the Asian monsoon (Williamson et al., 2026). Due to the closer proximity to surface sources, higher aerosol load reaches the upper troposphere in this region. Secondary maxima can be seen around 10°N in the tropics, and at around 40°S. The latter represents lofting of aerosol particles by e.g., warm conveyor belts (e.g., Jo et al., 2025; Joppe et al., 2025) in the Southern hemispheric storm tracks. A similar feature also exists in the Northern hemisphere, but is partially obscured by the strong maximum of the Tibetan plateau.

In the Northern hemisphere, a crossing of the extinction gradient and the tropopause can be detected. This can be a consequence of cross-tropopause transport by several mixing processes such as overshooting convection over the tropopause (e.g., Homeyer

https://doi.org/10.5194/egusphere-2026-6438
Preprint. Discussion started: 11 November 2026
© Author(s) 2026. CC BY 4.0 License.

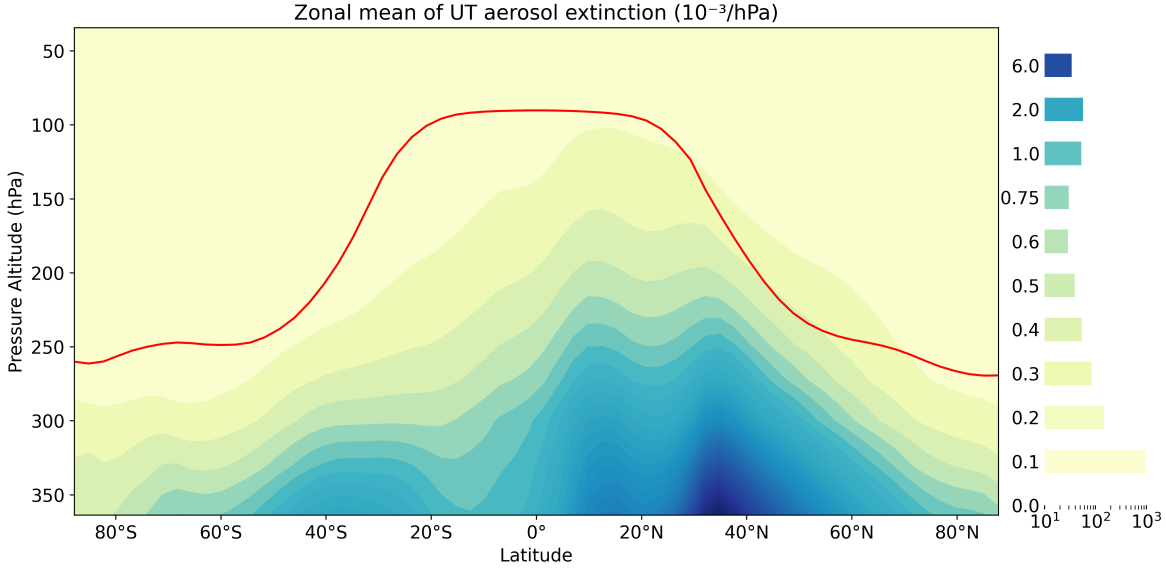


Figure 2. Zonal mean of the time-averaged UT extinction in 10^{-3}/hPa between 50 and 350 hPa. The red line marks the time and zonal average of the tropopause altitude. The color bar depicts the frequency of occurrence for each extinction value.

and Bowman, 2021), clear-air-turbulence (e.g., Chau et al., 2025, 2026) or gravity wave induced mixing (e.g., Lachnitt et al., 2023), e.g., with the pathway via the Asian monsoon (e.g. Williamson et al., 2026).

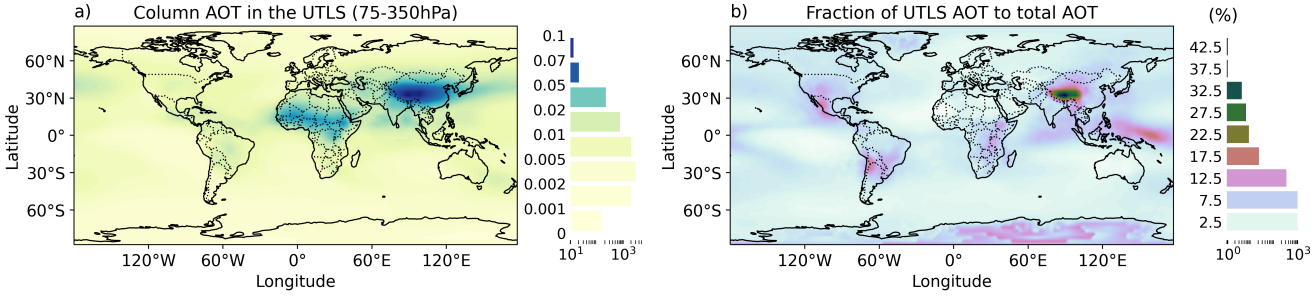


Figure 3. Panel a) denotes the spatial distribution of the column UT AOT between the pressure levels of 75 and 350 hPa. Panel b) visualises the fraction of the UT column AOT to the total AOT. Note, that the color bars also represent the frequency of occurrence for each value (without area weighting) on a logrithmic scale.

Even though the absolute values for the extinction are relatively small, the vertical column integral over the UT region between 75 and 350 hPa, can reach non-negligible values, as depicted the left panel in Fig. 3. The majority of the values are rather low (median at around 0.005), however, there are certain regions where the UT column AOT reaches a value of up to 0.1. Those are the regions already identified in Fig. 2, namely the Tibetan plateau with influences of the Asian monsoon and

https://doi.org/10.5194/egusphere-2026-6438
Preprint. Discussion started: 11 November 2026
© Author(s) 2026. CC BY 4.0 License.

the sub-Sahel region in Africa, where regularly mesoscale convective systems can transport aerosol particles up to the UTLS or newly formed particles from precursor material contribute to enhanced aerosol loading (e.g., Borrmann et al., 2010). Slightly elevated values are also found over the Amazon and in the midlatitude storm tracks (partially related to outflow from the Asian monsoon, e.g., Kaumanns et al., 2026).

Fig. 3b depicts the contribution of the UT AOT to the total AOT, indicating in which regions the UT aerosol has a potentially important impact on the radiation budget. Besides the region of the Asian monsoon, parts of the Southern Pacific Convergence Zone (SPCZ), over South America, Mexico and the Southern US, parts of South-East Africa and Antarctica show fractions larger than 10 % of the total AOT. In some of those regions, the total extinction is quite low, such that relative contributions easily exceed certain threshold values; however, other regions also stand out in Fig. 3a, indicating the relevance of the UT aerosol extinction for the energy budget of the Earth. Beside the obvious maxima, in more than 40 % of the grid boxes (note the logarithmic scale of the frequency distribution), between 5 and 10 % of the total AOT is located in the UT region.

3.1.3 UT aerosol extinction speciation

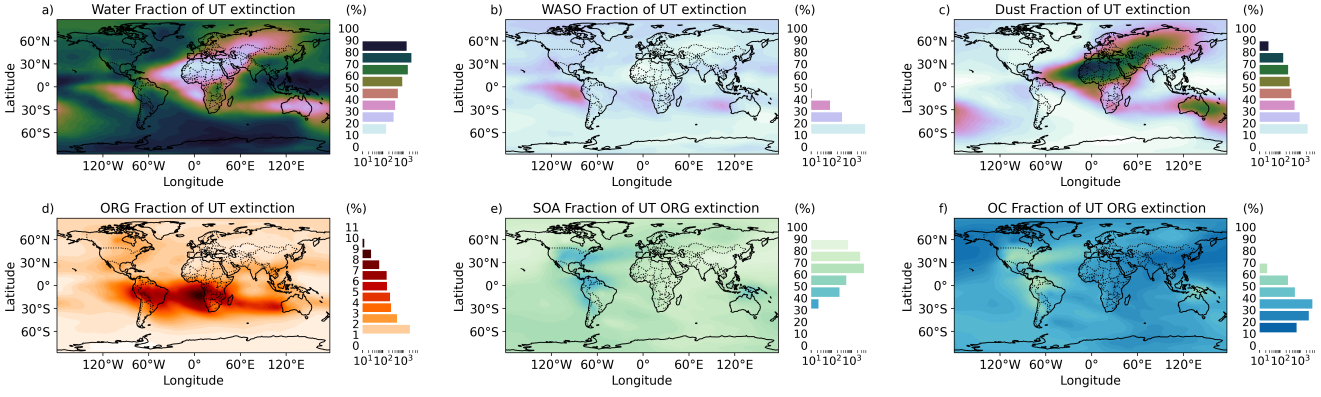


Figure 4. Spatial distribution of the UT column AOT at 550 nm fractional contribution of selected aerosol compounds. Panel a) depicts aerosol water, b) water soluble ions (mainly SO_4^{2-}, NO_3^- , and NH_4^+, abbreviated as WASO) c) mineral dust, and d) organic carbon (ORG). Panels e) and f) depict the SOA and combustion OC fraction of the total organics contribution. Note, that the color bars also show the frequency of occurrence on a logarithmic scale for each fraction (without area weighting).

To analyse, which species are most relevant for the UT extinction, a species weighted distribution of the UT column AOT is analysed. For this purpose, the volume fractions of the individual compounds, which also determined the mean refractive index is calculated and the total UT extinction is scaled with this volume fraction. This is displayed in Fig. 4.

The most important compound is aerosol water (panel a) of Fig. 4), usually contributing more than 60 to 70 % of the total extinction (see the frequency distribution of fractions in the color bar of Fig. 4a). This is related to the fact that many aerosol particles are very hygroscopic, e.g., sulphates, nitrates, ammonium, sea salt and to a minor degree also some organics. Consequently, growth factors from water uptake are often found between 1.5 and 2 (e.g., Clegg et al., 2019) at relative humidities

https://doi.org/10.5194/egusphere-2026-6438
Preprint. Discussion started: 11 November 2026
© Author(s) 2026. CC BY 4.0 License.

typical for the UTLS. The second most important component are WAter SOluble inorganic ions (abbreviated as "WASO"), i.e., mostly sulphates, nitrates and ammonium. Typically, 10 to 20 % of the extinction originates from those species (see panel b) of Fig.4), which are relevant for both aerosol nucleation as well as aerosol growth by condensation.

Mineral dust is the third important component (panel c) of Fig. 4, showing an anti-correlated pattern to the water contribution to the UT extinction. This is a consequence of the mostly hydrophobic behaviour of mineral dust (i.e., in the model mineral dust does not contribute to water uptake, only potential coating material takes up water), such that in regions of high dust loading in the UT, the fraction of water is reduced, whereas the mineral dust itself efficiently contributes to the mean refractive index. The regions, which show a high contribution from dust are located in the vicinity of the dust source regions. As indicated already in the analysis of Fig. 1, the dust load in the model most likely is overestimated, such that also the UT dust contribution is too high. Kohl et al. (2026) have reduced the UT dust bias by using a different size discretisation in the model; however, this approach had not been applied in this model configuration as it has not yet been finalised during the simulations for this study. Even though the color scaling in Fig. 4c shows a prominent effect of the dust, the overall frequency distribution indicates that in many regions dust only is a minor contributor to total UT aerosol extinction. Note that the absolute magnitude of the extinction can be derived from Fig. 5 which shows that in most latitude bands the dust contribution is smaller or of similar importance than for WASO components.

Fig. 4d depicts the contribution of organic material to the UT extinction. Given the production regions for SOA material over the tropical rainforests, a transport of SOA and their precursors in tropical convection without a complete wet removal (e.g., Bardakov et al., 2022) into the UT region and further downwind transport explains the patterns of the maxima of organic UT extinction contributions. Globally, the organic fraction is mostly on the order of only 1 to 2 %, but can locally reach up to 10 %. Panels e) and f) of Fig. 4 show that in most regions SOA dominates the UT organics contribution, except for continental US, Western Europe and the Northern part of South America. Those regions are either dominated by fossil fuel and/or biomass burning OC emissions and the subsequent transport into the UT. Biomass burning also plays a certain role over the Amazon showing that up to 30 % of the organic UT extinction originates from non-SOA species. As the contribution from SOA compounds dominates the organic contributions, the respective refractive indices and their effect are analysed in Sect. 3.4. Even though the SOA is treated in a highly simplified approach in this study, i.e., as a non-volatile compound, such a simplified treatment for secondary organics is often used in climate simulations, where less focus is on the actual phase partitioning of the organic material, but more on its climatic impact (Mann et al., 2014; Tsigaridis et al., 2014). The non-volatile fraction of SOA is on the order of 3.1 Tg (Shrivastava et al., 2015), which is represented in this study. Thus, the presented contribution of SOA to the total extinction represents a lower estimate of a potential overall effect.

Fig. 5 summarises the individual species contributions to the UT extinction on a logarithmic scale as a zonal mean. Given that scaling (linear scaling is depicted in the supplement Fig. S1) it becomes obvious that black carbon, organics and sea salt play minor roles for UT extinction on the global scale. Note that the organic fraction is more important in the low latitudes whereas sea salt has some relevance in the Southern storm track. The most important spcies are mineral dust, the water soluble ions and aerosol water. Note, that this result is only valid for the extinction: for absorbance BC and OC (especially from fossil fuels and biomass burning) play a more important role.

https://doi.org/10.5194/egusphere-2026-6438
Preprint. Discussion started: 11 November 2026
© Author(s) 2026. CC BY 4.0 License.

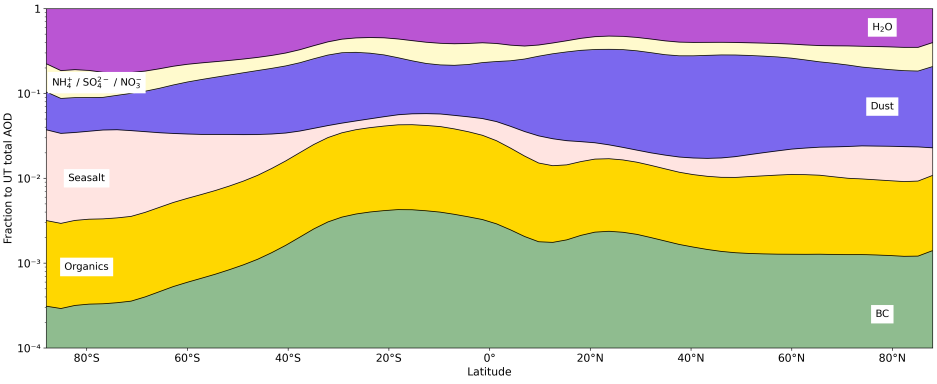


Figure 5. Multi-year mean of the cumulative fractions of the composition contributing to the UT column AOT. The x-axis depicts the latitude, whereas the y-axis shows the logarithm of the UT composition fractions. Note, that this logarithmic scaling allows to visualise also the low contributing species (e.g., BC), and over-proportionally displays their relevance compared to a linear scaling.

3.2 Implications for the radiation budget

To constrain the effect UT aerosols have on the radiation budget, this section depicts the response of the radiation fluxes to perturbance experiments. For this purpose, different scaling experiments of the UT extinction are analysed. The modified extinction directly affects the radiative transfer in the atmosphere. Note, that due to the design of the scaling experiments only direct aerosol-radiation interactions are investigated, and that there is no effect of the UT aerosol on cloud formation. Consequently, the radiative effects can be determined from one simulation alone with multiple calls to the radiation scheme, each with different aerosol extinction properties. Furthermore, only the extinction, but not the single scattering albedo or the asymmetry factor are modified in the scaling experiments. The scaling factors applied in the simulation are: 0.6, 0.9, 1.0, 1.1, 1.4 and 2.0. The resulting extinction zonal mean cross sections differences to the reference extinction value of 1.0 against altitude are shown in the supplementary material (Fig. S2) for four of the sensitivity cases.

Given those extinction values, the radiation at the surface is substantially modified. This is depicted in Fig.6. The panel a) shows the annual mean shortwave net flux at the surface. Given the optical properties of the UT aerosol, there is only a very weak longwave effect visible at the surface, such that the dominant effects in the lower troposphere can be attributed to the shortwave effects (see Fig. S6). The strongest difference (scaling effect minus reference) is found for panel b) for the scaling factor of 2.0. The substantially enhanced extinction in the UT leads to a maximum absolute shortwave disturbance of -0.48 W/m^2 in Central Africa in the sub-Sahel region. Additionally, a strong signal is obvious over the Tibetan plateau, which has already been identified as a region with high aerosol extinction in Sect. 3.1.2. In many mostly continental regions there is an effect between -0.1 and -0.2 W/m^2. Overall, the global mean effect (area weighted) is around -0.075 W/m^2, as the net shortwave flux is affected both by the aerosol, but much stronger by the incoming radiation flux at the top of the atmosphere with enhanced values over the tropics and reduced values in the high latitudes. Often the effect in the net shortwave flux is slightly smaller over the ocean due to the higher absorbance capacity of the ocean (lower albedo) (Chen et al., 2024). Given the low simulated

https://doi.org/10.5194/egusphere-2026-6438
Preprint. Discussion started: 11 November 2026
© Author(s) 2026. CC BY 4.0 License.

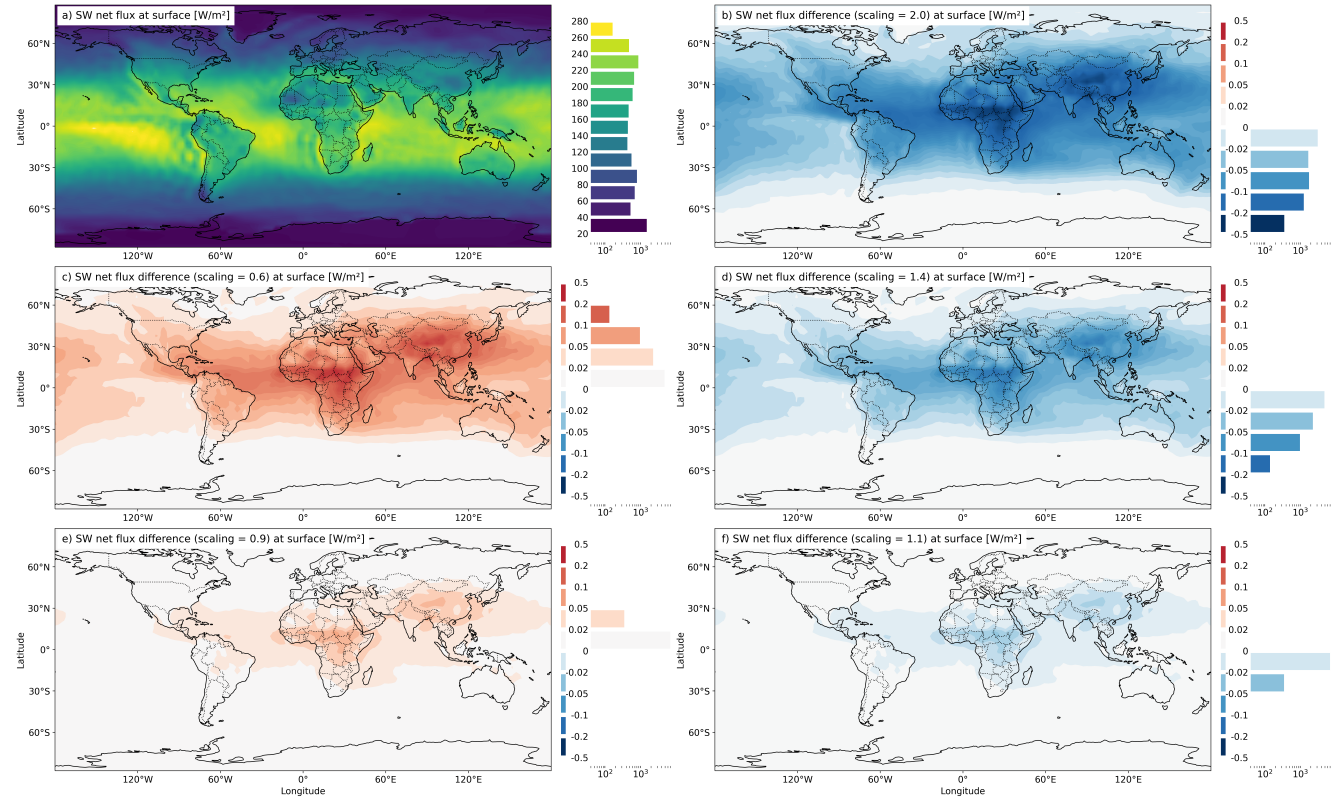


Figure 6. The panels depict the mean surface net shortwave radiation flux in W/m^2 (panel a)) and the respective absolute differences from the reference (flux from scaled extinction minus reference) for panels b) to f). The respective scaling factor for the UT extinction is provided in each panel. The color code also contains a (logarithmic) distribution of occurrence (without area weighting).

extinction values over the Southern Ocean and Antarctica in the UT, the scaling effects are very low in this region.

Panels c) and e) depict the radiative disturbance in the shortwave bands from a reduction of UT extinction. In those cases, the difference is globally positive. The two scaling sensitivities are smaller than the one in panel b) such that a weaker net effect is obtained. However, the regional patterns are very similar, as the spatial distribution of the UT extinction is not modified. Still, substantial regions with an absolute effect larger than 0.1 W/m^2 can be identified in panel c) with a scaling of 0.6. A similar pattern, but with opposite sign is depicted in panel d), showing the difference to the scaling factor of an enhancement of 40 %. Only for the low reduction factor of 0.9 the net shortwave effects are relatively small (Fig. 6e), and restricted to the tropics mostly, similarly to Fig. 6f with a 10 % enhancement, but the opposite signs.

The vertical distribution of the zonal mean fluxes shows both difference in latitude as well as in altitude (see Fig. S3).

Even though the maximum effects are relatively scarce (see respective frequency distributions in the color code panels of Fig 6), there is an overall global mean effect, which is depicted in Fig. 7. The solid lines represent the global (area weighted) average of the disturbances, including the variation with altitude. The semi-transparent areas around the solid lines mark

https://doi.org/10.5194/egusphere-2026-6438
Preprint. Discussion started: 11 November 2026
© Author(s) 2026. CC BY 4.0 License.

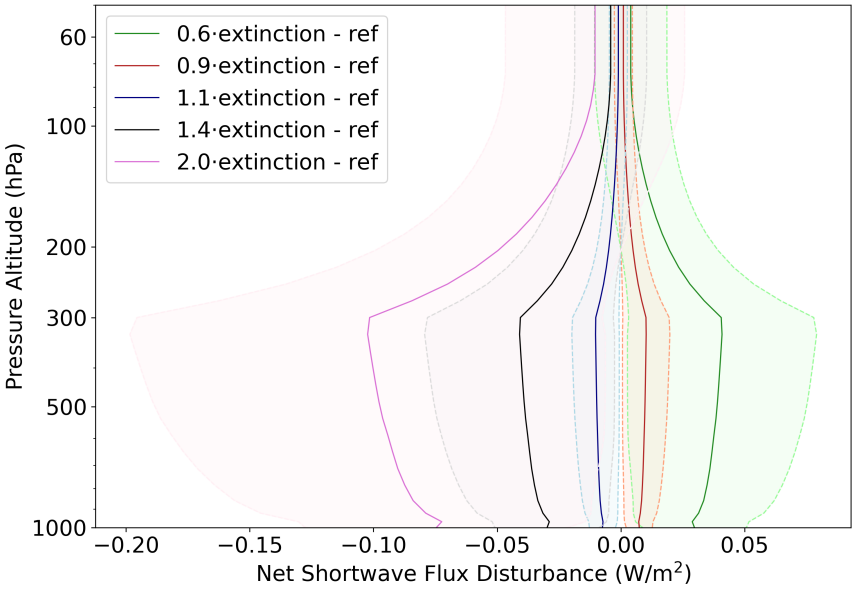


Figure 7. The graphic shows the vertical distribution of the global spatial mean net radiative shortwave disturbance originating from the scaling effects. The solid lines mark the difference of the shortwave fluxes in the respective scaling experiments minus the reference. 1σ areas are shaded in the corresponding colors UT. The different colors mark the individual differences as provided by the legend.

the area of 1σ standard deviation. The overall strongest effect is found for the scaling factor of 2.0 and then symmetrical distributions are found for the pairs of 1.4 and 0.6, and 1.1 and 0.9, respectively. The strongest net effect in the shortwave flux disturbance is around 300 hPa altitude, which marks the lower limit of the extinction scaling altitude. Above the upper limit of 80 hPa an overall reduced net shortwave flux is obvious for the scaling values larger than 1 (most strongly pronounced for the 2.0 scaling), which states that a fraction of the solar radiation is directly scattered backwards into space, therefore representing an enhanced shortwave upward flux. Analysing the upward shortwave fluxes (Fig. S4), both this increase above the enhanced aerosol layer is similar obvious as the change of sign from above to below the aerosol enhancement. The reduction of UT extinction leads to a reduced upward flux, as more radiation bypasses the UT and can be absorbed at the surface. The effect of surface reflection is still relevant despite the low planetary albedo. The area between 300 hPa and the surface shows a weakening of the (absolute) signals, which originate mostly from those surface effects. As can be seen from the supplementary material (Fig. S5), the clear sky fluxes show a very similar picture to the all sky fluxes, such that clouds can be ruled out as major contributors for shaping the profiles. Nevertheless, the clouds dampen the overall effects, as the enhanced backward scattering by the clouds is directly proportional to the incoming fluxes. Additionally, the cloud effects are identical in all simulations (total cloud backward scattering).

The overall longwave effects (Fig. S6) become mainly visible in the UT, and especially above, as they enhance the upward (and therefore also the net) flux into space for scaling values larger than 1. In the lower troposphere, the shortwave effects clearly

https://doi.org/10.5194/egusphere-2026-6438
Preprint. Discussion started: 11 November 2026
© Author(s) 2026. CC BY 4.0 License.

dominate the signal, whereas in the stratosphere shortwave and longwave effects almost cancel out. This is partly a result of the fact that there is no feedback between the modified radiative fluxes and the dynamics and the corresponding temperature distribution.

3.3 Implications for surface temperature

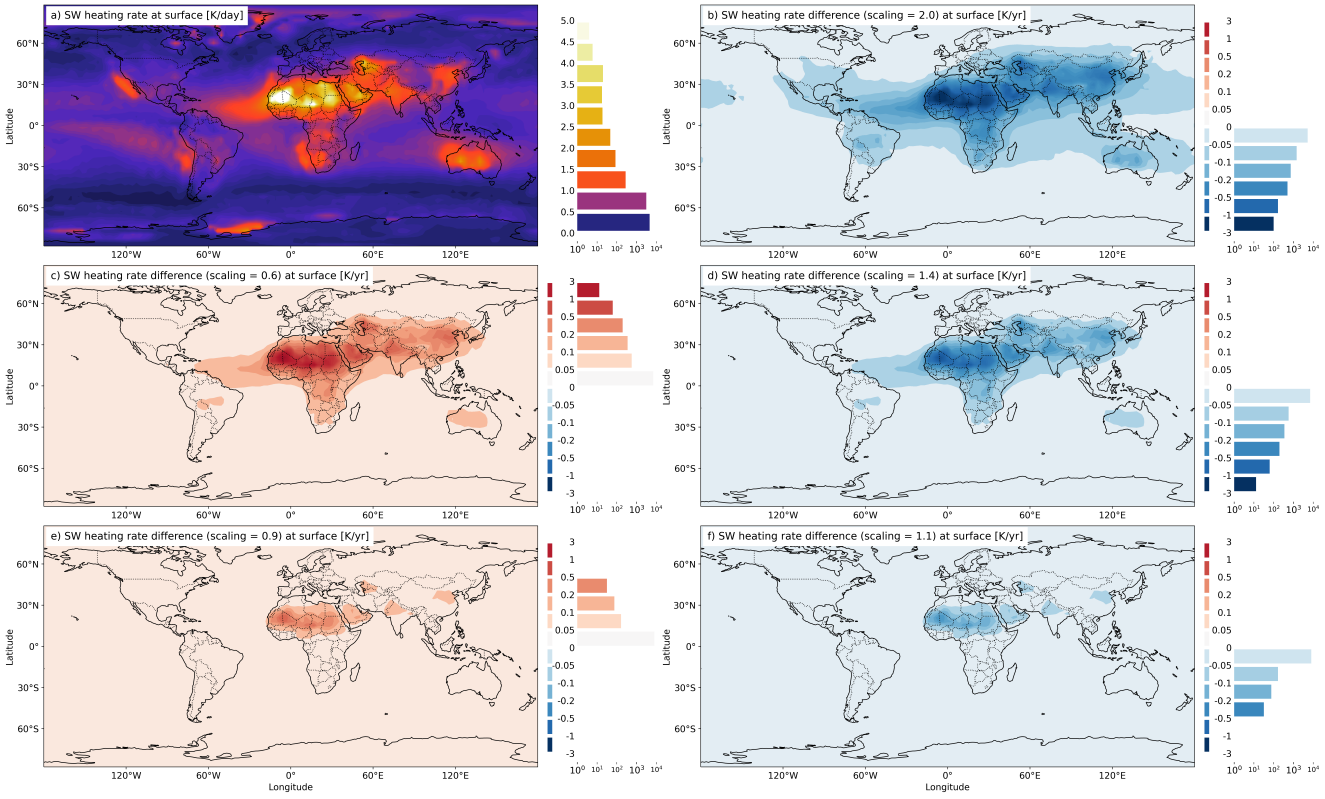


Figure 8. Panel a) shows the surface shortwave heating rate (K/day) for the reference extinction and the panels b) to f) visualise the differences for the scaled extinction calculations, i.e., scaled minus reference in K/yr. Panels c) and e) depict the effects for the reduced AOT (factor 0.6 and 0.9, respectively), whereas b), d) and f) show the effects of an enhanced UT AOT (factor 2.0, 1.4, and 1.1, respectively). Note that the color bars also denote the frequency of occurrence for the individual values on a logarithmic scale (without area weighting).

The shortwave radiative fluxes at the surface also directly affect the temperature distribution on Earth. Consequently, the corresponding heating rates and the effects of the UT extinction are quantified in Fig. 8. Instead of a direct temperature change, panel a) shows the surface heating rates from the shortwave influence. As seen from Fig. S6 the longwave effect near the surface is negligible, such that the shortwave heating corresponds to the total surface heating. The maximum heating occurs in the low latitudes and mostly over the continents, especially Africa, The Arabian peninsula, India, China and Australia. The majority of the heating (non-area weighted) is below 1 K/day, but in some regions values of up to 5 K/day heating are simulated.

https://doi.org/10.5194/egusphere-2026-6438
Preprint. Discussion started: 11 November 2026
© Author(s) 2026. CC BY 4.0 License.

The panels b) to f) show the changes of those heating rates from the reference (Fig. 8a). Note, that the unit of those changes is provided in K/yr, such that the changes are in the percentage range of the reference heating rates. As expected, the heating rate is enhanced for the scaling experiments which result in a higher net shortwave flux (panel c) and e) of Fig. 6 and Fig. 7). On the other hand, the reduction of the net shortwave flux originating from increased UT extinction propagates directly into reduced heating rates near the surface (panel b), d) and f) of Fig. 6 and Fig. 7). However, the patterns of those differences do not match those from the net shortwave surface flux perfectly, but are folding those changes with the amplitude of the maximum heating rates. Especially, for the weaker extinction disturbance the changes are relatively small, mostly below the 0.1 % threshold. In absolute values, as depicted in Fig. 7, those changes appear not important, but they are significant on the 95 % threshold.
Furthermore, the net surface flux changes of $\sim$ 0.1 W/m^2 are of similar magnitude as e.g., the climate effects of contrails with values of $\sim$ 100 mW/m^2 (e.g., Petzold et al. (2025), even though in their study effective radiative forcings are provided). Compared to the global warming changes of 3.5 to 4 W/m^2 from greenhouse gases and total -1.3 W/m^2 from aerosol cooling (Forster et al., 2021), the contribution of the UT aerosol appears relevant, especially if it is altered by natural or anthropogenic influences, as indicated by scaling experiments.

3.4 The role of refractive indices for organics and their implications

As mentioned in Sect. 2.1.3 compared to previous model simulations with EMAC (e.g., Pozzer et al., 2015) the optical properties for organic carbon have been separated into a contribution from secondary organic compounds (from the biosphere) and organics from burning processes (anthropogenic and biomass burning emissions). For the burning emissions, a higher absorbing fraction is used, as provided by Sutherland and Khanna (1991), whereas for SOA optical properties according to Liu et al. (2016) are selected. As shown in Fig. 4, especially in the UT the majority of organic carbon is SOA, such that these changes will impact the radiative properties of the UT, but also the total aerosol effects. These are analysed in this section. The findings are summarised in Fig. 9 which depicts the differences of the "old" treatment where all organic carbon utilised the refractive indices based on Sutherland and Khanna (1991) minus the separated refractive indices for SOA and OC from burning processes. Panel a) shows the effect of the modified refractive indices in extinction in the shortest radiation band (300 to 700 nm wavelength). As the extinction depends to a strong part on the real part of the refractive index, and this one is only slightly altered, the effect on the extinction is relatively low, between -0.04 to -0.6 %. This is also shown in Fig. 1d, i.e., a slight reduction in extinction becomes visible. However, the strongest effect becomes obvious in the UTLS region, even above the tropopause in the vicinity of the subtropical jet, where material can be transported from the troposphere to the stratosphere. However, absolute values for extinction are relatively small in this region.
A stronger effect of up to 2 % (absolute) is simulated for the single scattering albedo, showing the absorption properties of the aerosol particles in the same wavelength band (Fig 9b). The negative changes, which are due to the reduction of absorption by applying the more scattering coefficients for SOA, cause the absorption not only in the UT, but all over the tropical troposphere to be reduced (which means that the single scattering albedo is enhanced towards more scattering in the new formulation).
This has certain effects on the short wave net fluxes, which are shown in the zonal mean in panel c) of Fig. 9, and in the net surface shortwave flux (Fig 9e). Above 600 hPa, both in the troposphere and in the stratosphere, the net shortwave flux is

https://doi.org/10.5194/egusphere-2026-6438
Preprint. Discussion started: 11 November 2026
© Author(s) 2026. CC BY 4.0 License.

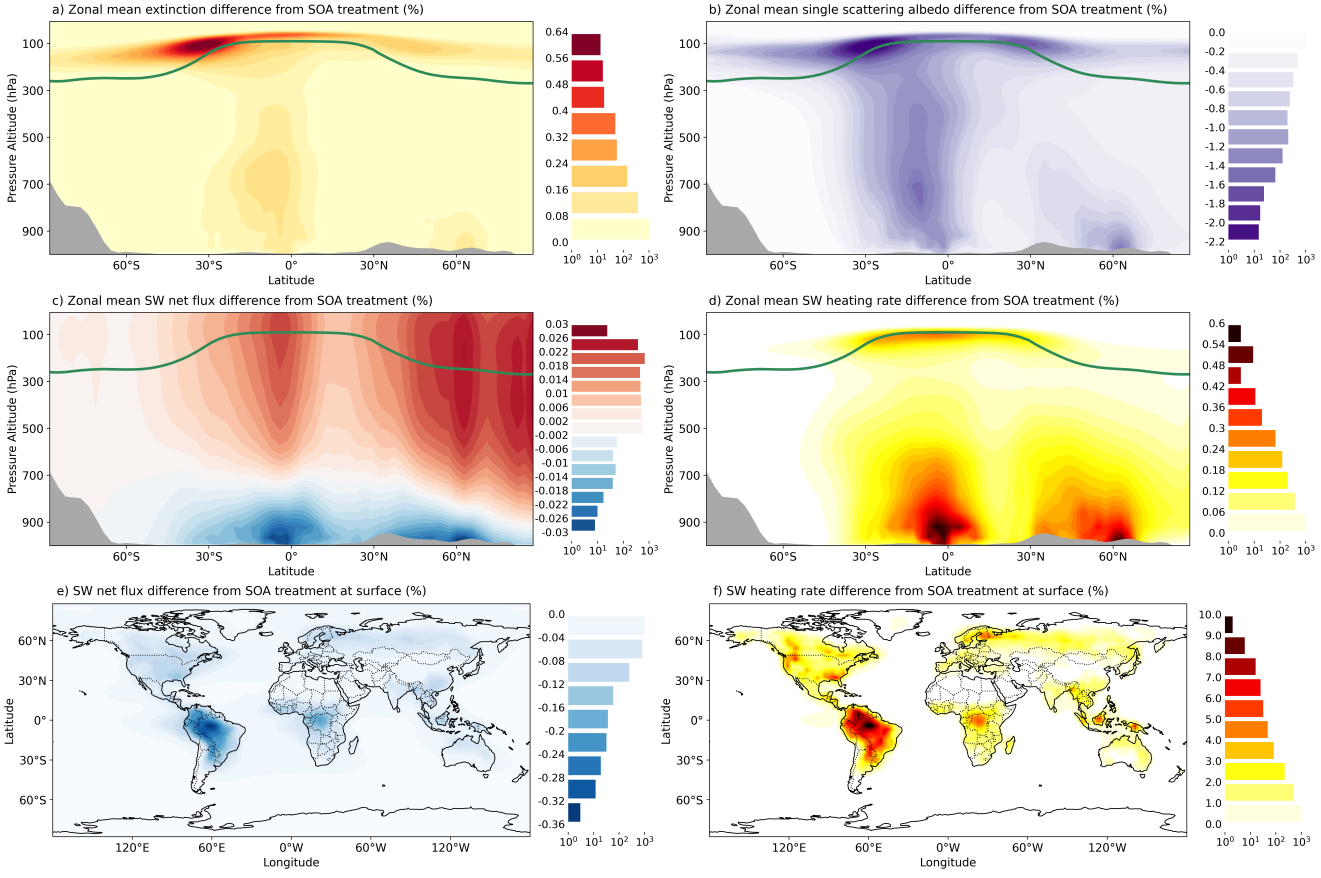


Figure 9. This figure displays the percentage changes in a) zonal mean extinction, b) zonal mean single scattering albedo, c) zonal mean net shortwave flux d) zonal mean shortwave heating rate, e) Surface net shortwave radiative flux and f) surface heating rate. The differences (in %) are calculated from the "old" approach (with identical parameters for all organic carbon) minus the "new" approach with separated SOA and burning OC optical properties. Note that the color bars denote the unweighted frequency of occurrence for all grid cells (after averaging), respectively.

enhanced if SOA is separated from burning OC, whereas in the lower troposphere the net flux is reduced. The relative contributions in the zonal mean are below 0.03 %, but show a systematic picture with strongest effects mostly originating from the UTLS. At the surface, locally the changes in the net surface flux can reach more than 0.3 %, which in the Amazon correspond to $\sim$ 0.6 W/m^2 radiation flux difference. The effects are strongest in the tropics, i.e., over tropical rainforests, which exhibit the highest mixing ratios of SOA due to the biogenic emissions of SOA precursors. However, weaker effects are also visible in other (mostly continental regions) where enhanced SOA from biogenic activity is produced and located.

The resulting differences in the radiation are also translated into changes in heating rates (see panels d) and f) of Fig. 9). Panel d) shows the zonal mean vertical heating rate differences, which in the tropics and the Northern hemisphere midlatitudes results in changes of 0.5 % in the zonal mean. Another heating change is located in the tropical tropopause region. Due to the

https://doi.org/10.5194/egusphere-2026-6438
Preprint. Discussion started: 11 November 2026
© Author(s) 2026. CC BY 4.0 License.

lower aerosol load in the UT, the effect on heating rates is consequently weaker at the elevated altitude. The pattern of high values in the planetary boundary layer and enhancement in the UT is typical for the active convection in the low latitudes, which is able to partially transport either SOA or less soluble precursor material to elevated altitude (see e.g., Tripathi et al., 2025; Curtius et al., 2024). Near the surface, this heating can have a very strong local effect, as seen over the Amazon. There, changes of almost up to 10 % in the heating rate are simulated if the SOA is treated identical to burning OC compared to the reduced absorption for SOA. Further pronounced signals are found in regions with a high SOA load, such as Central Africa, the maritime continent, Finland, but also some regions of the US and Canada with about half the signal strength compared to Amazonia. Although the overall effect is not large, the new separation should be maintained, as such effects are relevant for SOA-related vegetation–climate interactions in EMAC simulations (Vella et al., 2023). In some climate-change scenarios, such as reforestation, neglecting this separation could even lead to the wrong sign of the simulated response, i.e., warming instead of cooling (Vella et al., 2025).

4 Conclusions

This study analyses the effects of aerosol optical properties on the radiation and resulting temperature in the troposphere. An updated and extended submodel (AOP) for aerosol optical properties has been developed and applied in the global chemistry-climate model EMAC. AOP retains all capabilities of AEROPT while providing additional functionality, including support for the PSrad radiation (Nützel et al., 2024) scheme with online aerosols, which was not previously available. While AOP and AEROPT do not produce bitwise-identical results, the resulting differences are not scientifically significant. Furthermore, several recent technical developments have been implemented exclusively for AOP. This includes e.g., an option for a flexible incorporation of different refractive indices and additional radiatively active compounds to consider, such as volcanic ash, brown carbon or meteoric or space debris material.

Results from multi-year mean simulations are presented in this manuscript. The simulation results show that the UT column AOT is on the order of $\sim$ 5 %, but can locally contribute up to more than 30 % of the total AOT. The major contributors to the UT extinction are aerosol water and water soluble inorganic ions. In arid regions in the vicinity of the deserts, also lofted mineral dust can contribute significantly to the total extinction (even though potentially the simulated lofted dust burden might be overestimated). Organics play a secondary role for the UT extinction, even though in some regions values exceeding 10 % are simulated. For the organics, SOA compounds dominate the UT organic carbon fractions.

Additionally, the sensitivity of the radiative fluxes to enhanced or reduced extinction in the UT has been explored with the help of scaling experiments, all driven with the identical meteorology with multiple calls to the radiation code and scaled optical properties; however, there is no feedback from the scaling calculations via the diagnosed heating rates to the temperature. The results from the scaling experiments are summarised in Fig. 10, which shows the effect of modified UT extinction. This graphic is a summary of the results of the previous section, linking both extinction and its impact.

The scaling experiments yield a change of the global mean UT column AOT from 0.0071 (for a scaling factor of 0.6) to a value of 0.0117 (for a scaling factor of 2.0). The linear scaling of the extinction results in a change of almost an order of magnitude

https://doi.org/10.5194/egusphere-2026-6438
Preprint. Discussion started: 11 November 2026
© Author(s) 2026. CC BY 4.0 License.

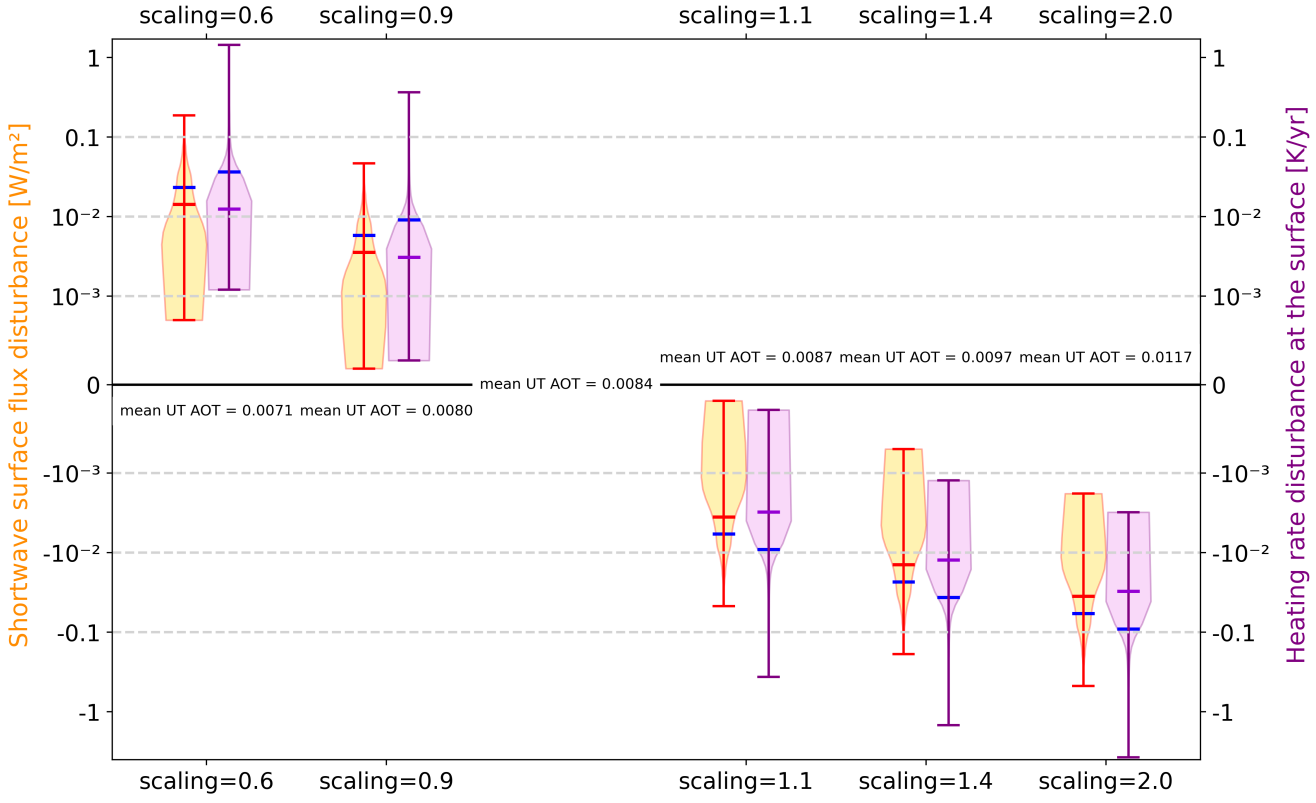


Figure 10. Violin plots of the surface radiation and temperature disturbances from UT aerosol modifications. Note that the violin plots are displayed on a symmetrical logarithmic scale. The corresponding scaling values and UT column AOT are depicted for the individual violins. The yellow violins depict the shortwave radiation surface flux differences and the violet violins the corresponding heating rates (both in absolute values). Mean values are given by the blue line, median values by the central bar in the respective violin bar colors. Note that all grid cells are used without area weighting.

differences in the radiative fluxes, i.e., from a few mW/m^2 to almost 100 mW/m^2 (note the logarithmic y-axis, such that there is no linear dependency). In addition to the near surface effects, the scaling has also implications for the vertical profile of the radiative fluxes (and corresponding) disturbances, i.e., that the strongest effects in the shortwave spectrum are found at the lower edge of the scaled region, whereas the longwave effects are increasing with height to the upper edge of the scaling region and are constant above to the top of the atmosphere. The longwave effects are smaller, than the shortwave effects in the troposphere.

An additional sensitivity test analysed the effect of a separation of SOA from combustion organics. It becomes obvious, that since a large fraction of the organics are SOA, the absorption of organics would be substantially estimated erroneously if only a single set of refractive indices for all organics would be used. Therefore, the distinction is relevant. This is going to be further

https://doi.org/10.5194/egusphere-2026-6438
Preprint. Discussion started: 11 November 2026
© Author(s) 2026. CC BY 4.0 License.

analysed in an upcoming study, taking the absorbing potential of different organics, especially so-called "brown carbon", into account.

Overall, the study shows that the optical properties of UT aerosols are important, as the UT extinction and absorption can have non-negligible impact both locally as well as on the surface climate. Even though the effects are smaller than for some trace gases (see Riese et al., 2012), changes in the UT aerosol load (e.g., from large forest fires, volcanoes, but also anthropogenic sources) can have a substantial impact on climate. Consequently, improved monitoring for aerosol components in the UTLS region should be goal for future missions such as e.g., the IAGOS initiative (Bundke et al., 2015), taking regular aerosol measurements in this sensitive region.

Code availability. The code for the AOP submodel is available via the MESSy repository. Currently applicants have to agree to the license for the EMAC model due to legacy code via the procedure described on the MESSy interface website (https://www.messy-interface.org). An open source release for the whole MESSy is currently in preparation. Additionally, the source code can be made available on request by contacting the authors of this manuscript.

Author contributions. HT developed the model code, conducted the model simulations and performed most of the analysis. MM contributed with the model configuration for this study. RV and DT prepared refractive index data sets. MK contributed by testing the new AOP code and contributed with comparisons to previous model versions and observations. MN and LS contributed to further extensions and generalisation of the model code and further testing. All co-authors contributed to the discussions and the manuscript draft.

Competing interests. There are no competing interests.

Acknowledgements. This work (HT, MM, MK) has received funding by the Deutsche Forschungsgemeinschaft (DFG, German Research Foundation) – TRR 301 “TPChange” (Project-ID 428312742).

This work used resources of the Deutsches Klimarechenzentrum (DKRZ) granted by its Scientific Steering Committee (WLA) under project ID 0893; we acknowledge the MESSy data pool, retained and globally distributed in the framework of the ESGF. The MESSy input data of this study were made available by the DKRZ.

We acknowledge the European Centre for Medium-Range Weather Forecasts (ECMWF) for providing the ERA5 reanalysis data, which was downloaded from the Copernicus Climate Data Store (CDS). The results contain modified Copernicus Climate Change Service information. Neither the European Commission nor ECMWF is responsible for any use that may be made of the Copernicus information or data it contains.

The MODIS Deep Blue aerosol products were retrieved from the Level-1 and Atmosphere Archive & Distribution System (LAADS) Distributed Active Archive Center (DAAC), NASA GSFC, Greenbelt, MD. We thank Dr. N. Christina Hsu (PI) and the Deep Blue science team

https://doi.org/10.5194/egusphere-2026-6438
Preprint. Discussion started: 11 November 2026
© Author(s) 2026. CC BY 4.0 License.



at NASA Goddard Space Flight Center (https://earth.gsfc.nasa.gov/climate/data/deep-blue) for providing the MODIS Deep Blue aerosol data
500 record.

The authors thank all the MESSy developers for support and contributions to a joint model development.

The graphics for this manuscript have been created with Python, using matplotlib, numpy and scipy packages.

https://doi.org/10.5194/egusphere-2026-6438
Preprint. Discussion started: 11 November 2026
© Author(s) 2026. CC BY 4.0 License.

References

Abdelkader, M., Stenchikov, G., Pozzer, A., Tost, H., and Lelieveld, J.: The effect of ash, water vapor, and heterogeneous chemistry on the evolution of a Pinatubo-size volcanic cloud, Atmospheric Chemistry and Physics, 23, 471–500, https://doi.org/10.5194/acp-23-471-2023, 2023.

Bardakov, R., Krejci, R., Riipinen, I., and Ekman, A. M. L.: The Role of Convective Up- and Downdrafts in the Transport of Trace Gases in the Amazon, Journal of Geophysical Research: Atmospheres, 127, e2022JD037 265, https://doi.org/10.1029/2022JD037265, e2022JD037265 2022JD037265, 2022.

Bohren, C. F. and Huffman, D. R.: Absorption and Scattering of Light by Small Particles, WILEY-VCH Verlag GmbH & Co. KGaA, https://doi.org/10.1002/9783527618156, 1998.

Borrmann, S., Kunkel, D., Weigel, R., Minikin, A., Deshler, T., Wilson, J. C., Curtius, J., Volk, C. M., Homan, C. D., Ulanovsky, A., Ravegnani, F., Viciani, S., Shur, G. N., Belyaev, G. V., Law, K. S., and Cairo, F.: Aerosols in the tropical and subtropical UT/LS: in-situ measurements of submicron particle abundance and volatility, Atmospheric Chemistry and Physics, 10, 5573–5592, https://doi.org/10.5194/acp-10-5573-2010, 2010.

Brock, C. A., Hamill, P., Wilson, J. C., Jonsson, H. H., and Chan, K. R.: Particle Formation in the Upper Tropical Troposphere: A Source of Nuclei for the Stratospheric Aerosol, Science, 270, 1650–1653, https://doi.org/10.1126/science.270.5242.1650, 1995.

Brühl, C., Lelieveld, J., Crutzen, P. J., and Tost, H.: The role of carbonyl sulphide as a source of stratospheric sulphate aerosol and its impact on climate, Atmospheric Chemistry and Physics, 12, 1239–1253, https://doi.org/10.5194/acp-12-1239-2012, 2012.

Bundke, U., Berg, M., Houben, N., Ibrahim, A., Fiebig, M., Tettich, F., Klaus, C., Franke, H., and Petzold, A.: The IAGOS-CORE aerosol package: instrument design, operation and performance for continuous measurement aboard in-service aircraft, Tellus B: Chemical and Physical Meteorology, 67, 28 339, https://doi.org/10.3402/tellusb.v67.28339, 2015.

Chau, C. H., Hoor, P., and Tost, H.: Simulated mixing in the UTLS by small-scale turbulence using multi-scale chemistry-climate model MECO(n), Atmospheric Chemistry and Physics, 25, 13 123–13 140, https://doi.org/10.5194/acp-25-13123-2025, 2025.

Chau, C. H., Hoor, P., Kaiser, K., and Tost, H.: Parametrizing the mixing by clear air turbulence in the chemistry climate model EMAC and its respective radiative impact, Atmospheric Chemistry and Physics, 26, 3637–3652, https://doi.org/10.5194/acp-26-3637-2026, 2026.

Chen, A., Zhao, C., Zhang, H., Yang, Y., and Li, J.: Surface albedo regulates aerosol direct climate effect, Nature Communications, 15, 7816, https://doi.org/10.1038/s41467-024-52255-z, 2024.

Clegg, S. L., Mazzoleni, L. R., Samburova, V., Taylor, N. F., Collins, D. R., Schum, S. K., and Hallar, A. G.: Modelling the hygroscopic growth factors of aerosol material containing a large water-soluble organic fraction, collected at the Storm Peak Laboratory, Atmospheric Environment, 214, 116 760, https://doi.org/10.1016/j.atmosenv.2019.05.068, 2019.

Curtius, J., Heinritzi, M., Beck, L. J., Pöhlker, M. L., Tripathi, N., Krumm, B. E., Holzbeck, P., Nussbaumer, C. M., Hernández Pardo, L., Klimach, T., Barmpounis, K., Andersen, S. T., Bardakov, R., Bohn, B., Cecchini, M. A., Chaboureau, J.-P., Dauhut, T., Dienhart, D., Dörich, R., Edtbauer, A., Giez, A., Hartmann, A., Holanda, B. A., Joppe, P., Kaiser, K., Keber, T., Klebach, H., Krüger, O. O., Kürten, A., Mallaun, C., Marno, D., Martinez, M., Monteiro, C., Nelson, C., Ort, L., Raj, S. S., Richter, S., Ringsdorf, A., Rocha, F., Simon, M., Sreekumar, S., Tsokankunku, A., Unfer, G. R., Valenti, I. D., Wang, N., Zahn, A., Zauner-Wieczorek, M., Albrecht, R. I., Andreae, M. O., Artaxo, P., Crowley, J. N., Fischer, H., Harder, H., Herdies, D. L., Machado, L. A. T., Pöhlker, C., Pöschl, U., Possner, A., Pozzer, A., Schneider, J., Williams, J., and Lelieveld, J.: Isoprene nitrates drive new particle formation in Amazon's upper troposphere, Nature, 636, 124–130, https://doi.org/10.1038/s41586-024-08192-4, 2024.

https://doi.org/10.5194/egusphere-2026-6438
Preprint. Discussion started: 11 November 2026
© Author(s) 2026. CC BY 4.0 License.



Dietmüller, S., Jöckel, P., Tost, H., Kunze, M., Gellhorn, C., Brinkop, S., Frömming, C., Ponater, M., Steil, B., Lauer, A., and Hendricks, J.: A new radiation infrastructure for the Modular Earth Submodel System (MESSy, based on version 2.51), Geoscientific Model Development, 9, 2209–2222, https://doi.org/10.5194/gmd-9-2209-2016, 2016.

Du, H.: Mie-scattering calculation, Appl. Opt., 43, 1951–1956, https://doi.org/10.1364/AO.43.001951, 2004.

Emde, C., Buras-Schnell, R., Kylling, A., Mayer, B., Gasteiger, J., Hamann, U., Kylling, J., Richter, B., Pause, C., Dowling, T., and Bugliaro, L.: The libRadtran software package for radiative transfer calculations (version 2.0.1), Geoscientific Model Development, 9, 1647–1672, https://doi.org/10.5194/gmd-9-1647-2016, 2016.

Forster, P., Storelvmo, T., Armour, K., Collins, W., Dufresne, J.-L., Frame, D., Lunt, D., Mauritsen, T., Palmer, M., Watanabe, M., Wild, M., and Zhang, H.: The Earth's Energy Budget, Climate Feedbacks, and Climate Sensitivity, p. 923–1054, Cambridge University Press, Cambridge, United Kingdom and New York, NY, USA, https://doi.org/10.1017/9781009157896.009, 2021.

Fountoukis, C. and Nenes, A.: ISORROPIA II: a computationally efficient thermodynamic equilibrium model for K^+-Ca^{2+}-Mg^{2+}-$NH_4{}^+$-Na^+-$SO_4{}^{2-}$-$NO_3{}^-$-Cl^--H_2O aerosols, Atmospheric Chemistry and Physics, 7, 4639–4659, https://doi.org/10.5194/acp-7-4639-2007, 2007.

Giles, D. M., Sinyuk, A., Sorokin, M. G., Schafer, J. S., Smirnov, A., Slutsker, I., Eck, T. F., Holben, B. N., Lewis, J. R., Campbell, J. R., Welton, E. J., Korkin, S. V., and Lyapustin, A. I.: Advancements in the Aerosol Robotic Network (AERONET) Version 3 database – automated near-real-time quality control algorithm with improved cloud screening for Sun photometer aerosol optical depth (AOD) measurements, Atmospheric Measurement Techniques, 12, 169–209, https://doi.org/10.5194/amt-12-169-2019, 2019.

Hernández Pardo, L., Curtius, J., Jöckel, P., Menken, J. M., Pöhlker, C., Pöhlker, M., and Possner, A.: Downward transport of tropical upper-tropospheric aerosols: multi-year insights from idealized simulations, Atmospheric Chemistry and Physics, 26, 12 275–12 293, https://doi.org/10.5194/acp-26-12275-2026, 2026.

Hersbach, H., Bell, B., Berrisford, P., Hirahara, S., Horányi, A., Muñoz-Sabater, J., Nicolas, J., Peubey, C., Radu, R., Schepers, D., Simmons, A., Soci, C., Abdalla, S., Abellan, X., Balsamo, G., Bechtold, P., Biavati, G., Bidlot, J., Bonavita, M., De Chiara, G., Dahlgren, P., Dee, D., Diamantakis, M., Dragani, R., Flemming, J., Forbes, R., Fuentes, M., Geer, A., Haimberger, L., Healy, S., Hogan, R. J., Hólm, E., Janisková, M., Keeley, S., Laloyaux, P., Lopez, P., Lupu, C., Radnoti, G., de Rosnay, P., Rozum, I., Vamborg, F., Villaume, S., and Thépaut, J.-N.: The ERA5 global reanalysis, Quarterly Journal of the Royal Meteorological Society, 146, 1999–2049, https://doi.org/10.1002/qj.3803, 2020.

Hess, M., Koepke, P., and Schult, I.: Optical Properties of Aerosols and Clouds: The Software Package OPAC, Bulletin of the American Meteorological Society, 79, 831 – 844, https://doi.org/10.1175/1520-0477(1998)079<0831:OPOAAC>2.0.CO;2, 1998.

Homeyer, C. R. and Bowman, K. P.: A 22-Year Evaluation of Convection Reaching the Stratosphere Over the United States, Journal of Geophysical Research: Atmospheres, 126, e2021JD034 808, https://doi.org/10.1029/2021JD034808, e2021JD034808 2021JD034808, 2021.

Jo, Y.-J., Jin, H.-G., Lee, H.-J., and Kim, C.-H.: The transport, removal, and formation of aerosols by a precipitating extratropical cyclone passing the Korean Peninsula, Atmospheric Research, 326, 108 323, https://doi.org/10.1016/j.atmosres.2025.108323, 2025.

Jöckel, P., Sander, R., Kerkweg, A., Tost, H., and Lelieveld, J.: Technical Note: The Modular Earth Submodel System (MESSy) - a new approach towards Earth System Modeling, Atmospheric Chemistry and Physics, 5, 433–444, https://doi.org/10.5194/acp-5-433-2005, 2005.

Jöckel, P., Kerkweg, A., Pozzer, A., Sander, R., Tost, H., Riede, H., Baumgaertner, A., Gromov, S., and Kern, B.: Development cycle 2 of the Modular Earth Submodel System (MESSy2), Geoscientific Model Development, 3, 717–752, https://doi.org/10.5194/gmd-3-717-2010, 2010.

https://doi.org/10.5194/egusphere-2026-6438
Preprint. Discussion started: 11 November 2026
© Author(s) 2026. CC BY 4.0 License.

Jöckel, P., Tost, H., Pozzer, A., Kunze, M., Kirner, O., Brenninkmeijer, C. A. M., Brinkop, S., Cai, D. S., Dyroff, C., Eckstein, J., Frank, F., Garny, H., Gottschaldt, K.-D., Graf, P., Grewe, V., Kerkweg, A., Kern, B., Matthes, S., Mertens, M., Meul, S., Neumaier, M., Nützel, M., Oberländer-Hayn, S., Ruhnke, R., Runde, T., Sander, R., Scharffe, D., and Zahn, A.: Earth System Chemistry integrated Modelling (ESCiMo) with the Modular Earth Submodel System (MESSy) version 2.51, Geoscientific Model Development, 9, 1153–1200, https://doi.org/10.5194/gmd-9-1153-2016, 2016.

Joppe, P., Schneider, J., Wilsch, J., Bozem, H., Breuninger, A., Curtius, J., Ebert, M., Emig, N., Hoor, P., Ismayil, S., Kandler, K., Kunkel, D., Kurth, I., Lachnitt, H.-C., Li, Y., Miltenberger, A., Richter, S., Rolf, C., Schneider, L., Schwenk, C., Spelten, N., Vogel, A. L., Cheng, Y., and Borrmann, S.: Transport of Biomass Burning Aerosol into the Extratropical Tropopause Region over Europe via Warm Conveyor Belt Uplift, Atmospheric Chemistry and Physics, 25, 15 077–15 103, https://doi.org/10.5194/acp-25-15077-2025, 2025.

Junge, C. E. and Manson, J. E.: Stratospheric aerosol studies, Journal of Geophysical Research (1896-1977), 66, 2163–2182, https://doi.org/10.1029/JZ066i007p02163, 1961.

Kaumanns, J., Ungermann, J., Vogel, B., Johansson, S., Kretschmer, E., Plöger, F., Preuße, P., Woiwode, W., and Riese, M.: Quantification of inmixing of Asian Monsoon air by multi-species classification in a match flight experiment, Atmospheric Chemistry and Physics, 26, 9083–9111, https://doi.org/10.5194/acp-26-9083-2026, 2026.

Kerkweg, A., Buchholz, J., Ganzeveld, L., Pozzer, A., Tost, H., and Jöckel, P.: Technical Note: An implementation of the dry removal processes DRY DEPosition and SEDImentation in the Modular Earth Submodel System (MESSy), Atmospheric Chemistry and Physics, 6, 4617–4632, https://doi.org/10.5194/acp-6-4617-2006, 2006a.

Kerkweg, A., Sander, R., Tost, H., and Jöckel, P.: Technical note: Implementation of prescribed (OFFLEM), calculated (ONLEM), and pseudo-emissions (TNUDGE) of chemical species in the Modular Earth Submodel System (MESSy), Atmospheric Chemistry and Physics, 6, 3603–3609, https://doi.org/10.5194/acp-6-3603-2006, 2006b.

Kinne, S., O'Donnel, D., Stier, P., Kloster, S., Zhang, K., Schmidt, H., Rast, S., Giorgetta, M., Eck, T. F., and Stevens, B.: MAC-v1: A new global aerosol climatology for climate studies, Journal of Advances in Modeling Earth Systems, 5, 704–740, https://doi.org/10.1002/jame.20035, 2013.

Kohl, M., Lelieveld, J., Chowdhury, S., Ehrhart, S., Sharma, D., Cheng, Y., Tripathi, S. N., Sebastian, M., Pandithurai, G., Wang, H., and Pozzer, A.: Numerical simulation and evaluation of global ultrafine particle concentrations at the Earth's surface, Atmospheric Chemistry and Physics, 23, 13 191–13 215, https://doi.org/10.5194/acp-23-13191-2023, 2023.

Kohl, M., Brühl, C., Tost, H., Xenofontos, C., Christoudias, T., Gromov, S., Appel, O., Borrmann, S., Bourassa, A., Campunzano-Jost, P., Cheng, Y., Eppers, O., Froyd, K. D., Holanda, B. A., Jimenez, J. L., Jöckel, P., Joppe, P., Kaiser, K., Katich, J. M., Klingmüller, K., Köllner, F., Kupc, A., Martin, A., Pöhlker, C., Pöhlker, M. L., Pöschl, U., Rieger, L., Ruhl, S., Schill, G. P., Schneider, J., Schulz, C., Schwarz, J. P., Tsimpidi, A. P., Vella, R., Williamson, C. J., Yang, Y., Zawada, D., Lelieveld, J., and Pozzer, A.: Global atmospheric aerosol distributions and composition from the Earth's surface to the stratosphere, EGUsphere, 2026, 1–54, https://doi.org/10.5194/egusphere-2026-3649, 2026.

Kremser, S., Thomason, L. W., von Hobe, M., Hermann, M., Deshler, T., Timmreck, C., Toohey, M., Stenke, A., Schwarz, J. P., Weigel, R., Fueglistaler, S., Prata, F. J., Vernier, J.-P., Schlager, H., Barnes, J. E., Antuña-Marrero, J.-C., Fairlie, D., Palm, M., Mahieu, E., Notholt, J., Rex, M., Bingen, C., Vanhellemont, F., Bourassa, A., Plane, J. M. C., Klocke, D., Carn, S. A., Clarisse, L., Trickl, T., Neely, R., James, A. D., Rieger, L., Wilson, J. C., and Meland, B.: Stratospheric aerosol—Observations, processes, and impact on climate, Reviews of Geophysics, 54, 278–335, https://doi.org/10.1002/2015RG000511, 2016.

https://doi.org/10.5194/egusphere-2026-6438
Preprint. Discussion started: 11 November 2026
© Author(s) 2026. CC BY 4.0 License.

Kumar, P., Vogel, H., Bruckert, J., Muth, L. J., and Hoshyaripour, G. A.: MieAI: a neural network for calculating optical properties of internally mixed aerosol in atmospheric models, npj Climate and Atmospheric Science, 7, 110, https://doi.org/10.1038/s41612-024-00652-y, 2024.

Lachnitt, H.-C., Hoor, P., Kunkel, D., Bramberger, M., Dörnbrack, A., Müller, S., Reutter, P., Giez, A., Kaluza, T., and Rapp, M.: Gravity-wave-induced cross-isentropic mixing: a DEEPWAVE case study, Atmospheric Chemistry and Physics, 23, 355–373, https://doi.org/10.5194/acp-23-355-2023, 2023.

Levy, R. C., Remer, L. A., and Dubovik, O.: Global aerosol optical properties and application to Moderate Resolution Imaging Spectroradiometer aerosol retrieval over land, Journal of Geophysical Research: Atmospheres, 112, https://doi.org/10.1029/2006JD007815, 2007.

Levy, R. C., Remer, L. A., Kleidman, R. G., Mattoo, S., Ichoku, C., Kahn, R., and Eck, T. F.: Global evaluation of the Collection 5 MODIS dark-target aerosol products over land, Atmospheric Chemistry and Physics, 10, 10 399–10 420, https://doi.org/10.5194/acp-10-10399-2010, 2010.

Levy, R. C., Mattoo, S., Munchak, L. A., Remer, L. A., Sayer, A. M., Patadia, F., and Hsu, N. C.: The Collection 6 MODIS aerosol products over land and ocean, Atmospheric Measurement Techniques, 6, 2989–3034, https://doi.org/10.5194/amt-6-2989-2013, 2013.

Liu, X., Ma, P.-L., Wang, H., Tilmes, S., Singh, B., Easter, R. C., Ghan, S. J., and Rasch, P. J.: Description and evaluation of a new four-mode version of the Modal Aerosol Module (MAM4) within version 5.3 of the Community Atmosphere Model, Geoscientific Model Development, 9, 505–522, https://doi.org/10.5194/gmd-9-505-2016, 2016.

Liu, Y., Huang, J., and Huang, F.: A Comprehensive Review on Study Methods of Aerosol Optical Properties in Different Dimensions, IEEE Access, 11, 36 763–36 786, https://doi.org/10.1109/ACCESS.2023.3266333, 2023.

Mahnke, C., Weigel, R., Cairo, F., Vernier, J.-P., Afchine, A., Krämer, M., Mitev, V., Matthey, R., Viciani, S., D'Amato, F., Ploeger, F., Deshler, T., and Borrmann, S.: The Asian tropopause aerosol layer within the 2017 monsoon anticyclone: microphysical properties derived from aircraft-borne in situ measurements, Atmospheric Chemistry and Physics, 21, 15 259–15 282, https://doi.org/10.5194/acp-21-15259-2021, 2021.

Mann, G. W., Carslaw, K. S., Reddington, C. L., Pringle, K. J., Schulz, M., Asmi, A., Spracklen, D. V., Ridley, D. A., Woodhouse, M. T., Lee, L. A., Zhang, K., Ghan, S. J., Easter, R. C., Liu, X., Stier, P., Lee, Y. H., Adams, P. J., Tost, H., Lelieveld, J., Bauer, S. E., Tsigaridis, K., van Noije, T. P. C., Strunk, A., Vignati, E., Bellouin, N., Dalvi, M., Johnson, C. E., Bergman, T., Kokkola, H., von Salzen, K., Yu, F., Luo, G., Petzold, A., Heintzenberg, J., Clarke, A., Ogren, J. A., Gras, J., Baltensperger, U., Kaminski, U., Jennings, S. G., O'Dowd, C. D., Harrison, R. M., Beddows, D. C. S., Kulmala, M., Viisanen, Y., Ulevicius, V., Mihalopoulos, N., Zdimal, V., Fiebig, M., Hansson, H.-C., Swietlicki, E., and Henzing, J. S.: Intercomparison and evaluation of global aerosol microphysical properties among AeroCom models of a range of complexity, Atmospheric Chemistry and Physics, 14, 4679–4713, https://doi.org/10.5194/acp-14-4679-2014, 2014.

Matus, A. V., L'Ecuyer, T. S., and Henderson, D. S.: New Estimates of Aerosol Direct Radiative Effects and Forcing From A-Train Satellite Observations, Geophysical Research Letters, 46, 8338–8346, https://doi.org/10.1029/2019GL083656, 2019.

Mie, G.: Beiträge zur Optik trüber Medien, speziell kolloidaler Metallösungen, Annalen der Physik, 330, 377–445, https://doi.org/10.1002/andp.19083300302, 1908.

Morgenstern, O., Hegglin, M. I., Rozanov, E., O'Connor, F. M., Abraham, N. L., Akiyoshi, H., Archibald, A. T., Bekki, S., Butchart, N., Chipperfield, M. P., Deushi, M., Dhomse, S. S., Garcia, R. R., Hardiman, S. C., Horowitz, L. W., Jöckel, P., Josse, B., Kinnison, D., Lin, M., Mancini, E., Manyin, M. E., Marchand, M., Marécal, V., Michou, M., Oman, L. D., Pitari, G., Plummer, D. A., Revell, L. E., Saint-Martin, D., Schofield, R., Stenke, A., Stone, K., Sudo, K., Tanaka, T. Y., Tilmes, S., Yamashita, Y., Yoshida, K., and Zeng, G.:

https://doi.org/10.5194/egusphere-2026-6438
Preprint. Discussion started: 11 November 2026
© Author(s) 2026. CC BY 4.0 License.

Review of the global models used within phase 1 of the Chemistry–Climate Model Initiative (CCMI), Geoscientific Model Development, 10, 639–671, https://doi.org/10.5194/gmd-10-639-2017, 2017.

Nützel, M., Stecher, L., Jöckel, P., Winterstein, F., Dameris, M., Ponater, M., Graf, P., and Kunze, M.: Updating the radiation infrastructure in MESSy (based on MESSy version 2.55), Geoscientific Model Development, 17, 5821–5849, https://doi.org/10.5194/gmd-17-5821-2024, 2024.

Pan, L. L., Atlas, E. L., Newman, P. A., Thornberry, T., Jucks, K. W., Toon, O. B., Randel, W. J., Liang, Q., Kinnison, D. E., Ueyama, R., Bresch, J. F., Honomichl, S. B., Smith, W. P., Hornbrook, R. S., Ziemba, L., Fujiwara, M., Apel, E. C., Barucci, M., Bianchini, G., Brown, M., Bui, T. P., Campos, T., Chin, M., D'Amato, F., Dean-Day, J., Diskin, G., Franchin, A., Gurganus, C., Iraci, L. T., Kim, J., Koo, J.-H., Lait, L. R., Lesko, K., Podolske, J. R., Rollins, A., Sakai, T., Shiraishi, K., Treadaway, V., Viciani, S., and Waxman, E.: The Asian Summer Monsoon Chemical and Climate Impact Project (ACCLIP): An Overview, Journal of Geophysical Research: Atmospheres, 130, e2025JD044 417, https://doi.org/10.1029/2025JD044417, e2025JD044417 2025JD044417, 2025.

Petzold, A., Khan, N. F., Li, Y., Spichtinger, P., Rohs, S., Crewell, S., Wahner, A., and Krämer, M.: Most long-lived contrails form within cirrus clouds with uncertain climate impact, Nature Communications, 16, 9695, https://doi.org/10.1038/s41467-025-65532-2, 2025.

Pincus, R. and Stevens, B.: Paths to accuracy for radiation parameterizations in atmospheric models, Journal of Advances in Modeling Earth Systems, 5, 225–233, https://doi.org/10.1002/jame.20027, 2013.

Plummer, D., Nagashima, T., Tilmes, S., Archibald, A., Chiodo, G., Fadnavis, S., Garny, H., Josse, B., Kim, J., Lamarque, J.-F., Morgenstern, O., Murray, L., Orbe, C., Tai, A., Chipperfield, M., Funke, B., Juckes, M., Kinnison, D., Kunze, M., Luo, B., Matthes, K., Newman, P. A., Pascoe, C., and Peter, T.: CCMI-2022: A new set of Chemistry-Climate Model Initiative (CCMI) Community Simulations to Update the Assessment of Models and Support Upcoming Ozone Assessment Activities, SPARC Newsletter, 57, 22–30, https://www.wdc-climate.de/ui/entry?acronym=ESCiMo2_SPARC57, 2021.

Pozzer, A., de Meij, A., Yoon, J., Tost, H., Georgoulias, A. K., and Astitha, M.: AOD trends during 2001–2010 from observations and model simulations, Atmospheric Chemistry and Physics, 15, 5521–5535, https://doi.org/10.5194/acp-15-5521-2015, 2015.

Pringle, K. J., Tost, H., Metzger, S., Steil, B., Giannadaki, D., Nenes, A., Fountoukis, C., Stier, P., Vignati, E., and Lelieveld, J.: Description and evaluation of GMXe: a new aerosol submodel for global simulations (v1), Geoscientific Model Development, 3, 391–412, https://doi.org/10.5194/gmd-3-391-2010, 2010.

Remer, L. A. and Kaufman, Y. J.: Dynamic aerosol model: Urban/industrial aerosol, Journal of Geophysical Research: Atmospheres, 103, 13 859–13 871, https://doi.org/10.1029/98JD00994, 1998.

Remer, L. A., Kaufman, Y. J., Tanré, D., Mattoo, S., Chu, D. A., Martins, J. V., Li, R.-R., Ichoku, C., Levy, R. C., Kleidman, R. G., Eck, T. F., Vermote, E., and Holben, B. N.: The MODIS Aerosol Algorithm, Products, and Validation, Journal of the Atmospheric Sciences, 62, 947 – 973, https://doi.org/10.1175/JAS3385.1, 2005.

Riese, M., Ploeger, F., Rap, A., Vogel, B., Konopka, P., Dameris, M., and Forster, P.: Impact of uncertainties in atmospheric mixing on simulated UTLS composition and related radiative effects, Journal of Geophysical Research: Atmospheres, 117, https://doi.org/10.1029/2012JD017751, 2012.

Roeckner, E., Brokopf, R., Esch, M., Giorgetta, M., Hagemann, S., Kornblueh, L., Manzini, E., Schlese, U., and Schulzweida, U.: Sensitivity of Simulated Climate to Horizontal and Vertical Resolution in the ECHAM5 Atmosphere Model, Journal of Climate, 19, 3771 – 3791, https://doi.org/10.1175/JCLI3824.1, 2006.

https://doi.org/10.5194/egusphere-2026-6438
Preprint. Discussion started: 11 November 2026
© Author(s) 2026. CC BY 4.0 License.

Rosanka, S., Tost, H., Sander, R., Jöckel, P., Kerkweg, A., and Taraborrelli, D.: How non-equilibrium aerosol chemistry impacts particle acidity: the GMXe AERosol CHEMistry (GMXe–AERCHEM, v1.0) sub-submodel of MESSy, Geoscientific Model Development, 17, 2597–2615, https://doi.org/10.5194/gmd-17-2597-2024, 2024.

Sander, R., Baumgaertner, A., Cabrera-Perez, D., Frank, F., Gromov, S., Grooß, J.-U., Harder, H., Huijnen, V., Jöckel, P., Karydis, V. A., Niemeyer, K. E., Pozzer, A., Riede, H., Schultz, M. G., Taraborrelli, D., and Tauer, S.: The community atmospheric chemistry box model CAABA/MECCA-4.0, Geoscientific Model Development, 12, 1365–1385, https://doi.org/10.5194/gmd-12-1365-2019, 2019.

Shrivastava, M., Easter, R. C., Liu, X., Zelenyuk, A., Singh, B., Zhang, K., Ma, P.-L., Chand, D., Ghan, S., Jimenez, J. L., Zhang, Q., Fast, J., Rasch, P. J., and Tiitta, P.: Global transformation and fate of SOA: Implications of low-volatility SOA and gas-phase fragmentation reactions, Journal of Geophysical Research: Atmospheres, 120, 4169–4195, https://doi.org/10.1002/2014JD022563, 2015.

Sutherland, R. A. and Khanna, R. K.: Optical Properties of Organic-based Aerosols Produced by Burning Vegetation, Aerosol Science and Technology, 14, 331–342, https://doi.org/10.1080/02786829108959495, 1991.

Tanre, D., Geleyn, J., and Slingo, J.: First results of the introduction of an advanced aerosol-radiation interaction in the ECMWF low resolution global model, in: Aerosols and their climatic effects, edited by Gerber, H. and Deepak, A., pp. 133 – 177, A. Deepak Hampton, Va., Meeting of Experts on Aerosols and their climatic effects, Williamsburg, Virginia, 28–30 March 1983, 1984.

Thomas, M. A.: Simulation of the climate impact of Mt. Pinatubo eruption using ECHAM5, Ph.D. thesis, University of Hamburg, Hamburg, https://doi.org/10.17617/2.994206, 2008.

Tost, H.: Chemistry–climate interactions of aerosol nitrate from lightning, Atmospheric Chemistry and Physics, 17, 1125–1142, https://doi.org/10.5194/acp-17-1125-2017, 2017.

Tost, H., Jöckel, P., Kerkweg, A., Sander, R., and Lelieveld, J.: Technical note: A new comprehensive SCAVenging submodel for global atmospheric chemistry modelling, Atmospheric Chemistry and Physics, 6, 565–574, https://doi.org/10.5194/acp-6-565-2006, 2006.

Tost, H., Lawrence, M. G., Brühl, C., Jöckel, P., Team, T. G., and Team, T. S.-O.-D.: Uncertainties in atmospheric chemistry modelling due to convection parameterisations and subsequent scavenging, Atmospheric Chemistry and Physics, 10, 1931–1951, https://doi.org/10.5194/acp-10-1931-2010, 2010.

Tripathi, N., Krumm, B. E., Edtbauer, A., Ringsdorf, A., Wang, N., Kohl, M., Vella, R., Machado, L. A. T., Pozzer, A., Lelieveld, J., and Williams, J.: Impacts of convection, chemistry, and forest clearing on biogenic volatile organic compounds over the Amazon, Nature Communications, 16, 4692, https://doi.org/10.1038/s41467-025-59953-2, 2025.

Tsigaridis, K., Daskalakis, N., Kanakidou, M., Adams, P. J., Artaxo, P., Bahadur, R., Balkanski, Y., Bauer, S. E., Bellouin, N., Benedetti, A., Bergman, T., Berntsen, T. K., Beukes, J. P., Bian, H., Carslaw, K. S., Chin, M., Curci, G., Diehl, T., Easter, R. C., Ghan, S. J., Gong, S. L., Hodzic, A., Hoyle, C. R., Iversen, T., Jathar, S., Jimenez, J. L., Kaiser, J. W., Kirkevåg, A., Koch, D., Kokkola, H., Lee, Y. H., Lin, G., Liu, X., Luo, G., Ma, X., Mann, G. W., Mihalopoulos, N., Morcrette, J.-J., Müller, J.-F., Myhre, G., Myriokefalitakis, S., Ng, N. L., O'Donnell, D., Penner, J. E., Pozzoli, L., Pringle, K. J., Russell, L. M., Schulz, M., Sciare, J., Seland, Ø., Shindell, D. T., Sillman, S., Skeie, R. B., Spracklen, D., Stavrakou, T., Steenrod, S. D., Takemura, T., Tiitta, P., Tilmes, S., Tost, H., van Noije, T., van Zyl, P. G., von Salzen, K., Yu, F., Wang, Z., Wang, Z., Zaveri, R. A., Zhang, H., Zhang, K., Zhang, Q., and Zhang, X.: The AeroCom evaluation and intercomparison of organic aerosol in global models, Atmospheric Chemistry and Physics, 14, 10 845–10 895, https://doi.org/10.5194/acp-14-10845-2014, 2014.

Vella, R., Forrest, M., Lelieveld, J., and Tost, H.: Isoprene and monoterpene simulations using the chemistry–climate model EMAC (v2.55) with interactive vegetation from LPJ-GUESS (v4.0), Geoscientific Model Development, 16, 885–906, https://doi.org/10.5194/gmd-16-885-2023, 2023.

https://doi.org/10.5194/egusphere-2026-6438
Preprint. Discussion started: 11 November 2026
© Author(s) 2026. CC BY 4.0 License.



Vella, R., Forrest, M., Pozzer, A., Tsimpidi, A. P., Hickler, T., Lelieveld, J., and Tost, H.: Influence of land cover change on atmospheric organic gases, aerosols, and radiative effects, Atmospheric Chemistry and Physics, 25, 243–262, https://doi.org/10.5194/acp-25-243-2025, 2025.

Waggoner, A. P., Weiss, R. E., Ahlquist, N. C., Covert, D. S., Will, S., and Charlson, R. J.: Optical characteristics of atmospheric aerosols, Atmospheric Environment (1967), 15, 1891–1909, https://doi.org/10.1016/0004-6981(81)90224-9, plumes and Visibility Measurements and Model Components, 1981.

Walker, J. S., Carruthers, A. E., Orr-Ewing, A. J., and Reid, J. P.: Measurements of Light Extinction by Single Aerosol Particles, The Journal of Physical Chemistry Letters, 4, 1748–1752, https://doi.org/10.1021/jz4008068, 2013.

Weigel, R., Mahnke, C., Baumgartner, M., Dragoneas, A., Vogel, B., Ploeger, F., Viciani, S., D'Amato, F., Bucci, S., Legras, B., Luo, B., and Borrmann, S.: In situ observation of new particle formation (NPF) in the tropical tropopause layer of the 2017 Asian monsoon anticyclone – Part 1: Summary of StratoClim results, Atmospheric Chemistry and Physics, 21, 11 689–11 722, https://doi.org/10.5194/acp-21-11689-2021, 2021.

Williamson, C. J., Kupc, A., Axisa, D., Bilsback, K. R., Bui, T., Campuzano-Jost, P., Dollner, M., Froyd, K. D., Hodshire, A. L., Jimenez, J. L., Kodros, J. K., Luo, G., Murphy, D. M., Nault, B. A., Ray, E. A., Weinzierl, B., Wilson, J. C., Yu, F., Yu, P., Pierce, J. R., and Brock, C. A.: A large source of cloud condensation nuclei from new particle formation in the tropics, Nature, 574, 399–403, https://doi.org/10.1038/s41586-019-1638-9, 2019.

Williamson, C. J., Borrmann, S., Brauner, P., Brock, C. A., Campos, T., Christoudias, T., D'Amato, F., Dragoneas, A., Eppers, O., Honomichl, S., Kohl, M., Köllner, F., Kupc, A., Lee, Y. R., Lyu, M., Michailoudi, G., Pan, L. L., Perring, A. E., Pozzer, A., Simone, D., Smith, W. P., Tost, H., Ueyama, R., Ullmann, K., Vakkari, V., Viciani, S., Virkkula, A., Weigel, R., Woods, S., and Xenofontos, C.: Upper troposphere aerosol formation enhanced by monsoon lofted pollution, Nature Communications, https://doi.org/10.1038/s41467-026-75073-x, 2026.

Wiscombe, W. J.: Improved Mie scattering algorithms, Appl. Opt., 19, 1505–1509, https://doi.org/10.1364/AO.19.001505, 1980.